Pricing and Scheduling Optimization Solutions in the Smart Grid

by

Binyan Zhao

B.Eng., Beijing University of Posts and Telecommunications, 2008

M.S., Beijing University of Posts and Telecommunications, 2011

A Dissertation Submitted in Partial Fulfillment of the

Requirements for the Degree of

DOCTOR OF PHILOSOPHY

in the Department of Electrical and Computer Engineering

Pricing and Scheduling Optimization Solutions in the Smart Grid

by

Binyan Zhao

B.Eng., Beijing University of Posts and Telecommunications, 2008

M.S., Beijing University of Posts and Telecommunications, 2011

Supervisory Committee

---

Dr. XiaoDai Dong, Supervisor

(Department of Electrical and Computer Engineering)

---

Dr. Jens Bornemann, Co-Supervisor

(Department of Electrical and Computer Engineering)

---

Dr. Henning Struchtrup, Outside Member

(Department of Mechanical Engineering)

**Supervisory Committee**

---

Dr. XiaoDai Dong, Supervisor

(Department of Electrical and Computer Engineering)

---

Dr. Jens Bornemann, Co-Supervisor

(Department of Electrical and Computer Engineering)

---

Dr. Henning Struchtrup, Outside Member

(Department of Mechanical Engineering)

## ABSTRACT

The future smart grid is envisioned as a large scale cyber-physical system encompassing advanced power, computing, communications and control technologies. In order to accommodate these technologies, it will have to build on solid mathematical tools which can ensure an efficient operation of such heterogeneous and emerging cyber-physical systems. This work provides comprehensive accounts of the application with optimization methods, probability theory, commitment and dispatching technologies for addressing open problems in three emerging areas that pertain to the smart grid: unit commitment, service restoration problems in microgrid systems, and charging services for the plug-in hybrid electric vehicle (PHEV) markets.

The work on the short-term scheduling problem in renewable-powered islanded microgrids is to determine the least-cost unit commitment (UC) and the associated dispatch, while meeting electricity load, environmental and system operating requirements. A novel probability-based concept, *probability of self-sufficiency*, is introduced to indicate the probability that the microgrid is capable of meeting local demand in a self-sufficient manner. Furthermore, we make the first attempt in approaching the mixed-integer UC problem from a convex optimization perspective, which leads to an analytical closed-form characterization of the optimal commitment and dispatch solutions.

The extended research of the renewable-powered microgrid in the connection mode is the second part of this work. In this situation, the role of microgrid is changed to be either an electricity provider selling energy to the main grid or a consumer purchasing energy from the main grid. This interaction with the main grid completes work on the scheduling schemes.

Third, a microgrid should be connected with the main grid most of the time. However, when a blackout of the main grid occurs, how to guarantee reliability in a microgrid as much as possible becomes an immediate question, which motivates us to investigate the service restoration in a microgrid, driven islanded by an unscheduled breakdown from the main grid. The objective is to determine the maximum of the expected restorative loads by choosing the best arrangement of the power network configurations immediately from the beginning of the breakdown all the way to the end of the island mode. The intermittency nature of the renewable power, as well as the uncertainty of the duration of the breakdown pose new challenges to this classic optimization scheduling task. The proposed two scenario-splitting methods can be solved in a two-step solving procedure, in which a Lagrangian technique and dynamic programming are utilized to provide an analytically sub-optimal yet efficient solution to the original problem.

Lastly, the work investigating the pricing strategy in future PHEV markets considers a monopoly market with two typical service classes. The unique characteristics of battery

charging result in a piecewise linear quality of service model. Resorting to the concept of subdifferential, some theoretical results, including the existence and uniqueness of the subscriber equilibrium as well as the convergence of the corresponding subscriber dynamics are established. In the course of developing revenue-maximizing pricing strategies for both service classes, a general tradeoff has been identified between monetization and customer acquisition.

# Contents

# List of Tables

# List of Figures

# ACKNOWLEDGEMENTS

First and foremost, I would like to express my gratitude to my supervisor, Prof. Xiaodai Dong for the continuous support of my Ph.D study and research, for her patience and inspired instructions, and providing me with an excellent atmosphere for doing research.

I also thank my Co-Supervisor, Prof. Jens Bornemann for his meticulous paper and thesis revision every time, and insightful suggestions and advice.

My sincere thanks also go to the my thesis outside committee member: Prof. Henning Struchtrup, for offering me valuable comments and questions.

I also thank my fellow classmates in the whole laboratory: Yi Shi, Zheng Xu, Ming Lei, Ping Cheng, Tong Xue, Le Liang, Weiheng Ni, Yongyu Dai, Leyuan Pan, Yuejiao Hui, Guowei Zhang, Wanbo Li, Yiming Huo, Farnoosh Talaei, for the research discussions and for all the fun we had in the last four years. Particularly, I am grateful to Dr. Yi Shi for enlightening me on the first glance of research.

Last but not least, I would like to thank my husband, Feng Hu. He is always cheering me up and stands by me through the good times and the bad. And my parents, who are always supporting me through my whole life.

*Binyan Zhao, Burnaby, BC, Canada*

# DEDICATION

To my parents,

My husband,

And all my friends,

Sow nothing, reap nothing.

# Chapter 1

# Introduction

## 1.1 Overview and Motivation

The smart grid is envisioned to be a large-scale cyber-physical system that can improve the reliability, efficiency of energy grids by integrating advanced techniques from diverse disciplines such as power systems, communications, signal processing, computing and mathematics. The smart grid is also regarded as essential technology paradigms that are able to address the worsening issues of global warming and dwindling fossil fuels that have posed great challenges to the maintenance of nations' energy infrastructure. This heterogeneous nature of the smart grid motivates the adoption of advanced technologies for overcoming the various challenges at different levels such as service design, control, dispatching and implementation.

In this context, an emerging power distribution system in the smart grid, known as microgrids, is quietly gaining momentum. A *microgrid* is an integrated system consisting of a set of distributed generators (microturbines (MTs), fuel cells (FCs), reciprocating engines) and renewable energy sources (solar photovoltaics (PVs) and wind turbine (WT) systems) that function cooperatively in parallel with, or autonomously of, the traditional electricity

*macrogrid*. This transparent adaptation in operational modes, along with the capacity to better manage distributed energy resources (DERs), renders microgrid the most promising solution to developing a more reliable and decentralized energy system. The challenge arises when the daily operation of a microgrid involves multiple generators cooperating to find the least operation cost dispatch while satisfying various technical, environmental and reliability constraints. Besides, the scheduling time in the control center cannot be too long due to the uncertainty nature of forecasted generation from renewable energy sources (RESs). This motivates us to deal with the unit commitment and scheduling problem in the autonomous microgrids from a convex optimization perspective, and meanwhile provides the practical contributions in determining the size of the energy storage systems. As an extension of the Unit Commitment (UC) scheduling of a microgrid in an "islanded mode", the interaction between the microgrid and the main grid should be addressed. Service restoration after a breakout is an old topic in the distribution power network, and in the context of microgrid to which the power supply from the main grid breaks unforseen, the unique features introduce further restrictions as well as simplifications to this classic optimization task.

The plug-in hybrid electric vehicle (PHEV) has shown great promise in replacing fuel-consuming vehicles and advancing the evolution of green energy, and becomes a critical part in the concept of smart grid. This will increase the load on the power grid from which the batteries of the PHEVs will be charged mostly. Besides, charging services will be necessary in satisfying the diverse needs from users purchasing the PHEVs. This motivates us to propose a pricing strategy for PHEVs' battery charging from a market perspective to support the PHEV to spread rapidly and healthily.

## 1.2 Research Issues

### 1.2.1 Short-Term Operation Scheduling in Renewable-Powered Microgrid (Islanded Mode)

The defining characteristic of a microgrid is its ability to separate itself seamlessly from the main grid during a utility grid disturbance, and function as a self-controlled entity with high efficiency and low greenhouse gas emissions. The unique features of microgrid introduce further restrictions as well as simplifications to the unit commitment and scheduling problem. Our work presents an efficient duality-based approach for this cost-optimal microgrid design (i.e., choice of generation components) under the constraints of emissions, operation, as well as aspects of reliability.

### 1.2.2 Short-Term Operation Scheduling in Renewable-Powered Microgrid (Connected Mode)

In our work, the unit commitment problem in a connected mode is formulated and solved with the similar method to the islanded case. The analysis focuses on the impacts from the interaction with the main grid. We will investigate and analyze the impact from the main grid under this case.

### 1.2.3 Service Restoration for a Renewable-Powered Microgrid in Unscheduled Island Mode

In the issue of service restoration in a microgrid, the restoration scheduling is to reconfigure the network by changing the topology of the distribution system through altering the open/closed status of switches. The objective is to find a combination of the switch states to cover as many loads as possible immediately from the beginning of the breakdown all the

way to the end of the island mode, on the premise that all constraints are met through the main grid's breakdown durations.

### 1.2.4 Pricing and Revenue Maximization for Battery Charging Services in PHEV Markets

PHEVs are anticipated to be widely adopted in the coming years. Building a widespread infrastructure, enabling battery charging at convenient locations such as road sides and parking lots, stands as a promising solution to enable broad adoption of PHEVs. The solution concept of charging stations plays an irreplaceable role over that of individual household charging. There are two types of charging services considered in the work, battery exchange service and battery charging service, which are currently envisioned to be implemented in the charging stations. Our work focuses on investigating the revenue-maximizing pricing strategies in a multi-class monopoly market for the charging service provider, meanwhile the requirements of the subscribers are satisfied.

## 1.3 Dissertation Organization

In Chapter 2, we consider a duality-based approach for the short-term operation scheduling in renewable-powered microgrids, which leads to an analytical closed-form characterization of the optimal commitment and dispatch solutions. The connected mode of renewable-powered microgrids is investigated as the extended work in Chapter 3. In Chapter 4, the service restoration problem of the renewable powered microgrid in an unscheduled breakdown is formulated and solved. Then, a pricing strategy to maximize the revenue in future PHEVs' battery charging services markets is discussed. Service models developed for a monopoly market with two typical service classes are given in Chapter 5. Finally, Chapter 6 concludes this dissertation.

## 1.4 Publications

Binyan Zhao, Yi Shi, Xiaodai Dong, Wenpeng Luan, and Jens Bornemann, "Short-Term Operation Scheduling in Renewable-Powered Microgrids: A Duality-Based Approach," *IEEE Trans. Sustainable Energy*, Vol 5, Issue 1, pp.209-217, Jan 2014.

Binyan Zhao, Yi Shi and Xiaodai Dong, "Pricing and Revenue Maximization for Battery Charging Services in PHEV Markets," *IEEE Trans. Vehicular Technology*, Vol 63, Issue 4, pp.1987-1993, May 2014.

Binyan Zhao, Xiaodai Dong, and Jens Bornemann, "Service Restoration for a Renewable-Powered Microgrid in Unscheduled Island Mode," *IEEE Trans. Smart Grid* , Vol 6, Issue 3, pp.1128-1136, May 2015.

# Chapter 2

# Short-Term Operation Scheduling in Renewable-Powered Microgrids (Islanded Mode)

Traditionally, the unit commitment problem is applied to large central generators in macrogrids, and some typical numerical methods are used to solve the optimal problem. In this chapter, we propose an analytical efficient duality-based approach to this problem, and provide theoretical analysis to verify its accuracy. The simulation results show that the proposed method not only renders no loss of optimality, but uses less processing time compared to the two classical methods.

## 2.1 Introduction and Motivation

The daily operation of a microgrid involves finding the least-cost dispatch of the distributed generators (DGs) that minimizes total operating cost, while meeting the electrical load as well as satisfying various technical, environmental and operating constraints. This can be seen as a downsized version of the unit commitment (UC) problem that is traditionally

applied to large central generators in macrogrids [1]. Mathematically, the UC task can be described as a mixed-integer optimization problem with a nonlinear solution space, which has been the subject of intensive investigation for more than 40 years (c.f., bibliographical survey [2]). Nevertheless, the unique features of microgrids introduce further restrictions as well as simplifications to this classic optimization task that need to be addressed.

The biggest challenge comes from the intermittent nature of renewable energy sources (RESs), which often leads to power variations and makes it much more difficult to produce accurate day-ahead schedules in microgrids. Therefore, operation scheduling of the dispatchable Distributed Generations (DGs) should be performed at a much finer level, providing quick and continuous power provision, based on the most recent and accurate forecasted data [3]. Secondly, while large thermal units are often subject to ramping rate limits that are typically in the order of several tens of megawatts per hour, it only takes several minutes for microturbines to ramp up from 0 to full load [4]. This further supports operation scheduling to be performed at a more granular level for microgrids [5]. Last but not least, the capacity of switching between different operational modes calls for a proper modeling framework that reflects the unique characteristic of microgrids.

Various numerical-based algorithms, including some typical heuristic methods, such as genetic algorithm (GA) [6, 7], particle swarm optimization (PSO) [8], simulated annealing techniques [9, 10], and network-flow programming [11] have been proposed to solve the optimal UC problem, but most of them only provide a reasonable numerical solution (suboptimal, nearly global optimal) and have high computational complexity. For the classical mixed-integer UC problem, the branch and bound (BB) technique provides accurate numerical results. However, the procedure is generally not efficient except when large portions of the solution space can be quickly discarded in the case that there are not too many solutions having near optimal function values. In [12], a linear optimization problem is formulated and numerically solved to determine the optimal size of Energy Storage System (ESS) that min-

imizes the operating cost. The authors in [13] and [5] also establish UC strategies based on piecewise linear blocks approximating the quadratic objective function and frequency droop scheme, respectively. The authors in [14] model explicitly the length of time the microgrid operates autonomously and use a Monte Carlo analysis to study the impact of RESs over a set of United Kingdom commercial load profiles.

This chapter deals with a quadratic formulation of the environmental/economic UC optimization problem in a microgrid that consists of DGs, RESs, and an ESS. The contributions of this work are summarized as follows: 1) in light of microgrid's unique operational feature and taking into account forecast errors that exist in demand and wind power forecast, a novel probability-based concept is proposed to indicate the probability that the microgrid is able to operate in islanded mode, termed "probability of self-sufficiency" (PSS); 2) the mixed-integer UC problem is approached from a convex optimization perspective, which leads to an analytical closed-form solution. Compared to two classical methods, branch and bound and genetic algorithm, the proposed method uses significantly less processing time yet renders no loss of optimality in performance; 3) the proposed method provides guidelines in deciding the size of the ESS to improve the autonomous target PSS for a microgrid efficiently.

Table 2.1: Nomenclature of Chapter 2

| Symbol | Description |
|---|---|
| $\alpha_{(.)},\ \beta_{(.)},\ \gamma_{(.)}$ | Emission coefficients of a unit |
| $\Delta_d$ | Demand forecast error |
| $\Delta_w$ | Wind power forecast error |
| $\epsilon$ | Convergence criterion parameter |
| $\lambda_{(.)}$, $\mu_{(.)}$, $\nu_{(.)}$ | Lagrange multipliers |
| $\mu_{e,d}$ | Mean of demand forecast error |
| $\mu_{e,w}$ | Mean of wind power forecast error |
| $\rho_{(.)}$ | Cooling time constant of a unit |
| $\sigma^2_{e,d}$ | Variance of demand forecast error |
| $\sigma^2_{e,w}$ | Variance of wind power forecast error |
| $\tau^{(.)}$ | Step size of the subgradient method |
| $\varphi_{(.)}$ | UC indication function |
| $\zeta$ | Emission limit |
| $[x]_b^a$ | Euclidean projection of $x$ to the interval $[a, b]$, i.e.,$[x]_b^a = \max(\min(x, a), b)$ |
| $(x)^+$ | Euclidean projection of $x$ to the interval $[0, +\infty)$, i.e., $(x)^+ = \max(x, 0)$ |
| $a_{(.)},\ b_{(.)},\ c_{(.)}$ | Fuel cost coefficients of a unit |
| $b'_{(.)},\ c'_{(.)}$ | Aggregated cost coefficients of a unit |
| $d_{(.)}$ | Maintenance cost coefficient of a unit |
| $erf(.)$ | Error function [15, Eqn. 8.250.1] |
| $i$ | Unit index (subscript) |
| $n$ | Iteration index (superscript) |
| $p_{(.)}$ | Power dispatch of a unit |
| $p^*_{(.)}$ | Optimal power dispatch of a unit |

| | |
|---|---|
| $p_{(.)}^{min},\ p_{(.)}^{max}$ | Minimum and maximum power generation limits |
| $p_w$ | Wind turbine power output |
| $\overline{p}_{(.)}$ | Power dispatch of a unit in the relaxed UC problem |
| $\widehat{p}_{w,t}$ | Forecasted wind power in time interval $t$ |
| $t$ | Hour index (subscript) |
| $u_{(.)}$ | Unit status indicator of a unit where 1 means on and 0 means off |
| $v_{in}$ | Cut-in wind speed |
| $v_{out}$ | Cut-out wind speed |
| $v_r$ | Rated wind speed |
| $v_w$ | Wind speed |
| $w_r$ | Rated electrical power |
| $A_t$ | Modified electricity demand in time interval $t$ |
| $BB$ | Branch and bound method |
| $C_{min},\ C_{max}$ | Lower and upper limits of the energy stored in ESS |
| $CSC_{(.)}$ | Cold start-up cost of a unit |
| $D(.)$ | Dual function |
| $D_t$ | Forecasted demand in time interval $t$ |
| $E_{(.)}$ | Emission function of a unit |
| $F_{\Delta_w}$ | CDF of wind power forecast error |
| $FC_{(.)}(.)$ | Fuel cost function of a unit |
| $GA$ | Generic algorithm |
| $HSC_{(.)}$ | Hot start-up cost of a unit |
| $\mathcal{L}(.)$ | Lagrange function |
| $MC_{(.)}(.)$ | Maintenance cost function of a unit |
| $MUT_{(.)}$,$MDT_{(.)}$ | The time a unit needs to remain on/off if on/off at the beginning of the scheduling period |

| | |
|---|---|
| $N$ | Total number of units |
| $P(.)$ | Probability operator |
| $PSS$ | Probability of self-sufficiency |
| $R_t$ | Operating reserve requirement in time interval $t$ |
| $STC_{(.)}$ | Start-up cost function of a unit |
| $T$ | Total time horizon of one day |
| $TC$ | Total cost of all units |
| $TU_{(.)}$,$TD_{(.)}$ | The time a unit has been on/off at the beginning of the scheduling period |

## 2.2 System Model

We consider a microgrid that consists of a set of $N$ DG units, including both MTs and FCs, a RES, the wind turbine, and an energy storage module, the ESS. Electrical loads in the microgrid are prioritized into tiers, which consist of, e.g., *critical loads* that relate to essential processes that must be always met and lower-priority *non-critical loads* that can be temporarily removed until adequate power is available. Due to the limited capacity of the DERs and as in [16, 17, 18], we assume that the microgrid schedules its units to meet the critical loads in the highest priority, satisfies the non-critical loads using best efforts, and purchases power from the macrogrid in case of supply shortage. Besides, to better utilize an environmental-friendly resource, we assume the WT is always on and functions as the primary power source [12]. The DGs, on the other hand, serve as backup generators and work collaboratively with the WT to meet the critical loads. The ESS module is introduced to mitigate the renewable power intermittencies and load mismatches. In this work, we assume that the microgrid updates its UC strategy every one hour[1], during which load and generation are considered constant. Parameters are listed in the Nomenclature in Table 2.1.

### 2.2.1 Forecasted Wind Power Model

Wind power is the electrical power generated by wind turbines, installed in locations with strong and sustained winds. In practice, the actual wind power $p_w$ almost entirely depends on the wind speed $v_w$ when other physical limitations are fixed or change relatively slow [12]. In principle, $v_w$ is a random variable and varies continuously over time. In this work, we assume that $v_w$ remains unchanged in one scheduling period (i.e., one hour), and can vary independently between different scheduling periods.

Extensive research has been done in developing wind forecasting models and approaches

[1]Depending on different application requirements, smaller updating intervals can be selected since the closed-form UC solutions can be computed fast.

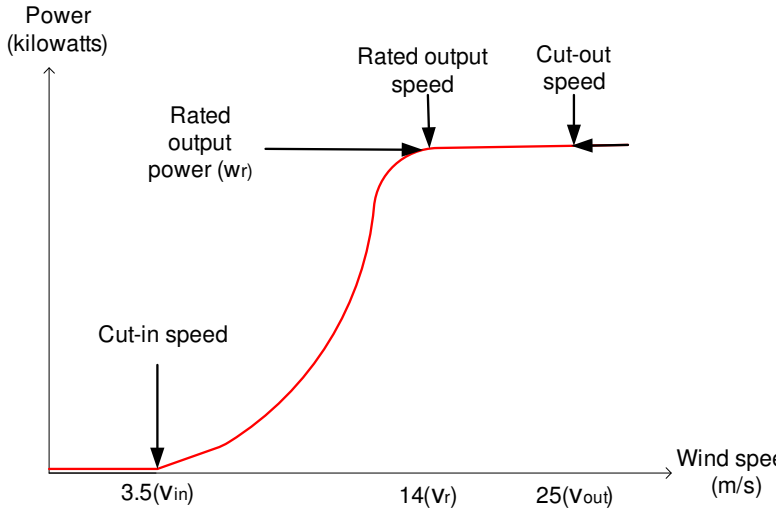


Figure 2.1: Wind power output versus the wind speed

[12, 19]. To capture the relationship between wind speed and wind power and as in [12, 20], the following piecewise linear model is adopted (c.f. Fig. 2.1)

$$p_w = \begin{cases} w_r & v_r \le v \le v_{out}, \\ \frac{(v-v_{in})w_r}{v_r - v_{in}} & v_{in} \le v < v_r, \\ 0 & \text{else.} \end{cases} \tag{2.1}$$

### 2.2.2 Cost Models for Microturbines and Fuel Cells

MTs are small electricity generators that burn gaseous and liquid fuels to create highspeed rotation that turns an electrical generator. Depending on the size range, an MT can ramp up from 0 to full load between 10 seconds to several minutes [4]. FC technology uses an electrochemical process rather than a combustion process to generate electricity. Polymer electrolyte FCs, also known as Proton Exchange Membrane (PEM) fuel cells, are particularly attractive for microgrids that require rapid start-up and quick response to load change [21].

The operating cost of an MT/FC usually includes fuel cost, maintenance cost, and start-up cost.

**Fuel Costs.** The fuel costs for DGs are considered as a quadratic model [22], which includes linear fuel cost models as special cases [12, 5]. The fuel costs of unit $i$ in time interval $t$ can be expressed as

$$FC_{i,t}(p_{i,t}) = a_i p_{i,t}^2 + b_i p_{i,t} + c_i. \tag{2.2}$$

**Maintenance Costs.** The maintenance costs for DGs are based on forecasts with minimal real-life situations, which are assumed to be proportional with the produced power [23]. Therefore, the maintenance cost of unit $i$ in time interval $t$ is

$$MC_{i,t}(p_{i,t}) = d_i p_{i,t}. \tag{2.3}$$

**Startup Costs.** The generator start-up cost depends on the time the unit has been off prior to a start-up. The start-up cost of unit $i$ in time interval $t$ can be represented by an exponential cost curve [22, Eqn. (3.12)]

$$STC_{i,t} = \left( HSC_i + CSC_i \left[ 1 - \exp\left( \frac{-TD_{i,t}}{\rho_i} \right) \right] \right) \cdot (1 - u_{i,t-1}). \tag{2.4}$$

Sometimes, the industry is interested in the total cost per day

$$TC = \sum_{t=1}^{T} \sum_{i=1}^{N} u_{i,t} \left( FC_{i,t} + MC_{i,t} + STC_{i,t} \right). \tag{2.5}$$

### 2.2.3 Emission Model

Emission effects should be taken into account for environmental friendly power production. The microgrids are envisioned to be new energy-saving and green grids in the future, which entails carbon emissions limited to regulations and law requirements.

The amount of emissions produced depends on fuel used, pollution control devices installed, and the amount of electricity generated. In this work, we assume that only DGs

produce emissions and the RESs are emission-free[2]. The emission function is typically expressed as a polynomial, the order of which depends on the desired accuracy [25, 26]. As in [13, 26], a quadratic function is considered for the emission curve as follows

$$E_{i,t}(p_{i,t}) = \alpha_i p_{i,t}^2 + \beta_i p_{i,t} + \gamma_i. \tag{2.6}$$

### 2.2.4 Energy Storage System

In renewable-powered microgrids, the problem of mitigating power intermittencies as well as load mismatches is an important and challenging task. In this context, the ESS plays a critical role in shaving peak demand and compensating forecast errors. For instance, when the forecasted wind power is smaller than the actual value (i.e., an underestimate), the supplied power is likely to be larger than the actual electricity demand, in which case the ESS will be functioning in the charging state to store surplus electrical/renewable energy, which can be dispatched properly later in the event of a power shortage.

The charge and discharge of the ESS is subject to stored energy limits, $C_{min}$ and $C_{max}$, which specify the minimum and maximum energy stored in the battery bank, respectively. In this case, $C_{max}$ is set as the full capacity of the ESS and $C_{min}$ to be around 10% of its full capacity. The ESS is also subject to starting and ending limits that specify the initial and final energy inside the battery bank during the course of one day. In this work, the starting and ending limits are both selected as $C_{min}$ for the purpose of energy balance of the energy storage system [12].

[2]Note that the emissions in the production process of wind turbines and other equipment [24] have not been considered.

### 2.2.5 Unit and Operation Constraints

**Maximum and Minimum Output Limits.** The output power of the DG in stable operation is restricted by its lower and upper limits as follows

$$p_i^{min} \leq p_{i,t} \leq p_i^{max}. \tag{2.7}$$

In our case, the minimum available power for the DGs are zero, i.e., the DG can be turned off when the output power from the WT is enough to meet the demanded power.

**Minimum Up/Down Time.** Once a DG is switched on, it has to operate continuously for a certain number of time before it can be switched off. Also, a certain number of hours has to pass before a DG can be brought online after being switched off. Violation of such constraints can shorten the unit's life time. Mathematically, we have

$$(TU_{i,t-1} - MUT_i)(u_{i,t-1} - u_{i,t}) \geq 0, \tag{2.8}$$

$$(TD_{i,t-1} - MDT_i)(u_{i,t} - u_{i,t-1}) \geq 0. \tag{2.9}$$

For DGs in microgrids, the minimum up/down time of DGs is around 600s and 300s [3], respectively, which is always satisfied under hourly scheduling operations.

**Ramp Rates.** Traditional thermal units are often subject to ramp rate limits that specify the amount a unit's generation can increase or decrease during one scheduling period. In the context of microgrids, small DG units can ramp up from 0 to full load in the order of several minutes [21]. Thus, ramp rate limits are typically not reached under normal hourly scheduling operations.

**Emission Limits.** To comply with the purpose of environment conservation and reduce the greenhouse gas footprint, we impose hourly emission limits on all the DGs. Mathematically,

we have

$$\sum_{i=1}^{N} u_{i,t} E_{i,t}(p_{i,t}) \leq \zeta. \tag{2.10}$$

**Operating Reserves.** In the event of a power supply disruption, operating reserve constraints guarantee that there exist extra generating capacity to the system that can be brought online immediately (spinning reserves) or within a short interval (supplementary reserves). In microgrids with fast-start DGs, operating reserves are imposed as follows [1]

$$\sum_{i=1}^{N} (p_i^{max} - u_{i,t} p_{i,t}) \geq R_t. \tag{2.11}$$

**Probability of Self-sufficiency.** Both demand and renewable power forecast are prone to errors, which affect negatively the microgrid in meeting local power demand and their autonomous and independent functions. Once a microgrid cannot meet power demand solely based on local generating units, it can switch to a grid-connected mode and purchase energy from the upstream macrogrid, and in our case we only consider the MG operating in the autonomous mode. To better understand the impacts of the operational mode on total operating cost, we propose the use of a novel probability-based concept, PSS, which indicates the target probability that the microgrid is able to operate in islanded mode without purchasing energy from the macrogrid.

As in [27, 28], we assume that both demand forecast error $\Delta_d$ and wind power forecast error $\Delta_w$ can be modeled as independent normally distributed random variables, i.e., $\Delta_d \sim N(\mu_{e,d}, \sigma_{e,d}^2)$ and $\Delta_w \sim N(\mu_{e,w}, \sigma_{e,w}^2)$. Then the probabilistic power balance constraint can be expressed as

$$P\left(\sum_{i=1}^{N} p_{i,t} u_{i,t} + \widehat{p}_{w,t} + \Delta_w \geq D_t + \Delta_d\right) \geq PSS, \tag{2.12}$$

which, after some algebra, can be reformulated as

$$\sum_{i=1}^{N} p_{i,t}u_{i,t} \geq A_t = D_t - \widehat{p}_{w,t} - \left((\mu_{e,w} - \mu_{e,d}) + \sqrt{2\left(\sigma_{e,w}^2 + \sigma_{e,d}^2\right)}erf^{-1}(1 - 2PSS)\right). \quad (2.13)$$

## 2.3 Problem Formulation and Closed-Form Solutions

### 2.3.1 Problem Formulation

The UC optimization problem in a particular operation scheduling interval $t$ can be written as

$$\begin{aligned} \textbf{P1} \qquad & \min_{\substack{p_{i,t},u_{i,t} \\ \forall i=1,...,N}} \quad \sum_{i=1}^{N} u_{i,t}\left(FC_{i,t} + MC_{i,t} + STC_{i,t}\right) \\ & \text{s.t.} \qquad (2.7) - (2.11) \text{ and } (2.13) \quad \forall i = 1, ..., N \end{aligned}$$

Evidently, problem **P1** is a mixed-integer programming problem with a nonlinear solution space. In order to transform **P1** into a convex optimization problem, we introduce auxiliary power variables $q_{i,t} = p_{i,t}u_{i,t}$ and relax $u_{i,t}$ to be a continuous variable in $[0, 1]$. Thus, the transformed problem can be written as[3]

$$\begin{aligned} \textbf{P2} \qquad & \min_{\substack{q_{i,t},u_{i,t} \\ \forall i=1,...,N}} \quad \sum_{i=1}^{N}\left(a_i q_{i,t}^2/u_{i,t} + b_i' q_{i,t} + c_{i,t}' u_{i,t}\right) \\ & \text{s.t.} \qquad \textstyle\sum_{i=1}^{N} q_{i,t} \geq A_t \\ & \qquad\quad \textstyle\sum_{i=1}^{N}\left(\alpha_i q_{i,t}^2/u_{i,t} + \beta_i q_{i,t} + \gamma_i u_{i,t}\right) \leq \zeta \\ & \qquad\quad \textstyle\sum_{i=1}^{N}(p_i^{max} - q_{i,t}) \geq R_t \\ & \qquad\quad u_{i,t}p_i^{min} \leq q_{i,t} \leq u_{i,t}p_i^{max}, \ \forall i = 1, ..., N \end{aligned}$$

[3]The objective function is defined at $u = 0$ by continuity as $\lim_{u\to 0}(aq^2/u + bq + cu) = 0$.

where the aggregated cost coefficients are $b'_i = b_i + d_i$ and $c'_{i,t} = c_i + STC_{i,t}$. Note that the objective function of **P2** is equivalent to that of **P1** as the change of variables is invertible except for $u_{i,t} = 0$. The same statement holds for the emission constraints (2.10) and (2.14). In case that $u_{i,t} = 0$, every $p_{i,t}$ solves **P1**.

The Hessian matrices of the objective function and the constraints of **P2** are positive semidefinite, and the form of the whole problem meets the requirement of a convex problem [29], implying that **P2** is a convex problem.

### 2.3.2 Closed-Form Solutions

To solve **P2** analytically, we first decouple the optimization variables $q_{i,t}$ and $u_{i,t}$ by substituting $\overline{p}_{i,t} := q_{i,t}/u_{i,t}$. Note that $\overline{p}_{i,t} = p_{i,t}$ for the case of interest, i.e., $u_{i,t} \neq 0$. For this reason, we will henceforth use $\overline{p}_{i,t} = p_{i,t}$. The Lagrangian function can then be written as

$$\mathcal{L}(\lambda_t, \mu_t, \nu_t, \mathbf{p}, \mathbf{u}) = \sum_{i=1}^{N} u_{i,t}\varphi_{i,t}(p_{i,t}) + \lambda_t A_t - \mu_t \zeta + \nu_t R_t - \nu_t \sum_{i=1}^{N} p_i^{max}, \tag{2.14}$$

where $\varphi_{i,t}(p_{i,t})$ can be viewed as the UC indication function

$$\varphi_{i,t}(p_{i,t}) = (a_i + \mu_t \alpha_i)p_{i,t}^2 + (b'_i + \mu_t \beta_i - \lambda_t + \nu_t)p_{i,t} + (c'_{i,t} + \mu_t \gamma_i). \tag{2.15}$$

The dual function can be obtained by minimizing the Lagrangian (2.14), which is given by

$$D(\lambda_t, \mu_t, \nu_t) = \min_{0 \leq u_{i,t} \leq 1} \sum_{i=1}^{N} u_{i,t} \min_{p_i^{min} \leq p_{i,t} \leq p_i^{max}} \varphi_{i,t}(p_{i,t}) + \lambda_t A_t - \mu_t \zeta + \nu_t R_t - \nu_t \sum_{i=1}^{N} p_i^{max}. \tag{2.16}$$

The initial step to solve (2.16) is to tackle the inner minimization, the solution of which can be easily derived as

$$p_{i,t}^{*} = \underset{p_i^{min} \le p_{i,t} \le p_i^{max}}{\arg\min} \varphi_{i,t}(p_{i,t}) = \left[ -\frac{b_i' + \mu_t \beta_i - \lambda_t + \nu_t}{2(a_i + \mu_t \alpha_i)} \right]_{p_i^{min}}^{p_i^{max}}. \tag{2.17}$$

The next step is to solve the outer minimization over $u_{i,t}$ in (2.16), given the optimal power dispatch solution (2.17). Evidently, the minimum value is attained by setting $u_{i,t} = 1$ for all $\varphi_{i,t}(p_{i,t}^{*}) < 0$ and $u_{i,t} = 0$ otherwise. Mathematically, we have

$$u_{i,t}^{*} = \begin{cases} 1 & \varphi_{i,t}(p_{i,t}^{*}) < 0, \\ 0 & \text{Otherwise.} \end{cases} \tag{2.18}$$

An important step in the course of analytical derivation is to decouple the optimizations of the commitment status $u_{i,t}$ and the power dispatch $p_{i,t}$ as in (2.16). Besides, we observe that the commitment decisions are completely determined by the sign of $\varphi_{i,t}(.)$ at the optimal dispatch $p_{i,t}^{*}$ (c.f. (2.18)). Thus, $\varphi_{i,t}(.)$ can be seen as a UC indication function. In the case that the power generated by the WT is sufficient to meet local power demand, the microgrid will be entirely powered by the RES and no DG needs to be turned on, i.e., $u_{i,t} = 0$ for all $i$.

So far, we have found the analytical optimal solutions $p_{i,t}^{*}$ in (2.17) and $u_{i,t}^{*}$ in (2.18), which are, however, functions of the Lagrangian multipliers. By convexity, it suffices to obtain the optimal dual variables ($\lambda_t^{*}$, $\mu_t^{*}$, $\nu_t^{*}$) to the dual problem, which are used to compute optimal primal solutions (2.17) and (2.18). The complete algorithm has be formally stated in **Algorithm 1** below.

This subsection discusses the use of a subgradient-based iterative procedure to numerically compute the corresponding optimal Lagrangian multipliers $\lambda_t^{*}$, $\mu_t^{*}$, and $\nu_t^{*}$. The key

**Algorithm 1** Subgradient-Based Algorithm

Initialize Lagrangian multiplier $\lambda_t^{(0)}$, $\mu_t^{(0)}$ and $\nu_t^{(0)}$ to arbitrary nonnegative values and set the step size $\tau^{(n)} = 1/(n+1)$.
**repeat**
  Compute economic dispatch $p_{i,t}^{*(n)}$ using (2.17).
  Obtain UC indication function $\varphi_{i,t}^{(n)}(p_{i,t}^{*(n)})$ via (2.15).
  Find unit status indicator $u_{i,t}^{*(n)}$ using (2.18).
  Update $\lambda_t^{(n+1)}$, $\mu_t^{(n+1)}$ and $\nu_t^{(n+1)}$ via (2.19), (2.20), and (2.21), respectively.
**until** $|TC^{(n)} - TC^{(n-1)}| < \epsilon\, TC^{(n-1)}$.

iteration steps are [29]

$$\lambda_t^{(n+1)} = \left[\lambda_t^{(n)} + \tau^{(n)} \left(A_t - \sum_{i=1}^{N} u_{i,t}^{*(n)} p_{i,t}^{*(n)}\right)\right]^{+}, \tag{2.19}$$

$$\mu_t^{(n+1)} = \left[\mu_t^{(n)} + \tau^{(n)} \left(\sum_{i=1}^{N} u_{i,t}^{*(n)} E_{i,t}\left(p_{i,t}^{*(n)}\right) - \zeta\right)\right]^{+}, \tag{2.20}$$

$$\nu_t^{(n+1)} = \left[\nu_t^{(n)} + \tau^{(n)} \left(R_t - \sum_{i=1}^{N} \left(p_i^{max} - p_{i,t}^{*(n)} u_{i,t}^{*(n)}\right)\right)\right]^{+}, \tag{2.21}$$

which are provably convergent to the optimal value provided that the step sizes are selected to satisfy $\sum_{n=1}^{\infty} \tau^{(n)} = \infty$ and $\sum_{n=1}^{\infty} \left(\tau^{(n)}\right)^2 < \infty$ [30]. A graphical convergence illustration can be found in the following simulation section.

## 2.4 Simulation Results and Discussion

In this study, a microgrid system consisting of two MTs, one FC, one WT, and one ESS is considered for a scheduling time horizon of 24 hours. The fuel cost coefficients, the emissions coefficients, and the power limits of the DGs are assumed to be known, with $p_{(.)}^{min}$ of all DGs are zero $kW$. Similar parameter settings have also been used in [6]. The emission limit $\zeta$ is set as 150 kg/hour. The wind speed data samples adopted in this work are from the "Wind Test Center" in West Texas A&M University [31], with the parameters in (2.1), $v_{in} = 3.5m/s, v_r = 14m/s, v_{out} = 25m/s$. Unless stated otherwise, the demand forecast

error statistics and those of the wind power are set as $\mu_{e,d} = \mu_{e,w} = 0$, $\sigma^2_{e,d} = 144$, and $\sigma^2_{e,w} = 256$. To understand the impact of PSS on the total operating cost, three different operation scenarios are considered, which are $PSS = 90\%$, $PSS = 70\%$, and $PSS = 50\%$.

### 2.4.1 Unit Commitment, Dispatching and Methods Comparison

This subsection shall illustrate the derived unit commitment solutions without considering the functionality of the ESS. The effects of the ESS will be investigated in Section 2.4.3. Fig. 2.2 illustrates the fast convergence behavior of the proposed algorithm in optimizing the total operating cost per day of the microgrid. It takes only about 20 iterations to reach the optimal solution under all three PSS values. Besides, observe from Fig. 2.2 that the operating cost increases as the microgrid functions more autonomously, since more power has to be generated to ensure self-sufficiency and to mitigate demand and wind power forecast errors.

Fig. 2.3 shows the comparison results of four different methods in our environmental/economic dispatch optimization problem. We use a GA and the proposed method (Prop-algor) to solve the original problem **P1** and the transformed problem **P2**, respectively. In addition, BB is applied to solve **P1**, providing us an accurate result as benchmark. The proposed method is shown to incur no loss of optimality, while GA is worse in terms of accuracy of the results. The optimal continuous results of **P2** given by the Matlab software cvx (CVX) are also close to the solution provided by BB and Prop-algor. CVX is used to solve convex problem, which also proves that **P2** is a convex problem from another perspective. More importantly, the simulation time of CVX, BB and GA are around 9 sec, 50 sec and 180 sec, respectively, while it only costs less than 3 sec for the proposed method to reach the same accuracy. The corresponding CPU time to run the proposed algorithm is plotted in Fig. 2.4. Observe that the algorithm running time decreases as the stopping criterion drops from within 0.1% of the value in the previous iteration to 10%. (The computer used was an ThinkPad Laptop with a i5 M560 duo-core processor at 2.67 GHz).

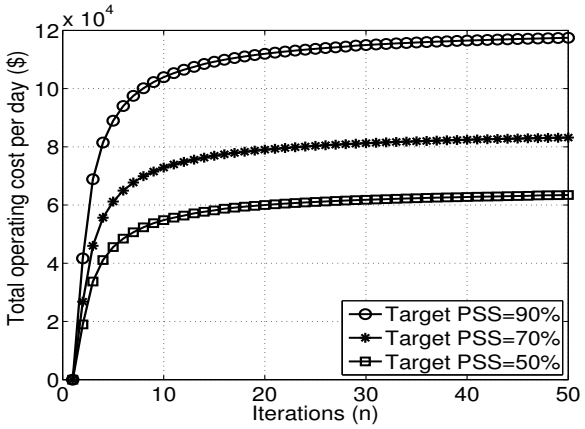


Figure 2.2: Total operating cost per day under different PSS targets.

The optimal amount of dispatch of each DG for given demand and wind power forecast profiles are shown in Fig. 2.5 under different target PSS values. Take Fig. 2.5(b) as an example. Observe the forecast wind power decreases from 1:00 am to 5:00 am in the early morning. In order to fulfill the demand, the DGs are dispatched economically according to the optimal UC solution. The dispatched power from the DGs continues to be in a higher level until 13:00 pm, when the forecast wind power comes into play again. At midnight, power demand reaches a minimum and the microgrid is entirely powered by the wind power. During the whole process, the DGs serve as backup sources that complement the renewable source in meeting electricity demand.

Table 2.2 further depicts the UC status of the DGs for the case of $PSS = 70\%$ over a period of 24 hours. Cross-referencing Fig. 2.5(b), we can observe that the FC is the most preferred power source among the DGs and contributes significantly during the entire scheduling period. In contrast, MT2 contributes the least and is always the last one to be turned on. The reason is as follows. Recall from Eqn. (2.18) in Section 2.3.2 that the commitment status of the DG is solely determined by the sign of the UC indication function $\varphi_{i,t}(.)$ at the optimal dispatched point $p^*_{i,t}$. An interesting phenomenon observed from numerical results is that $\varphi_{3,t}(p^*_{3,t}) < \varphi_{1,t}(p^*_{1,t}) < \varphi_{2,t}(p^*_{2,t})$ for all $t = 1, ..., T$. In other words, there exists a hidden *priority listing order* that arranges the DGs based on lowest

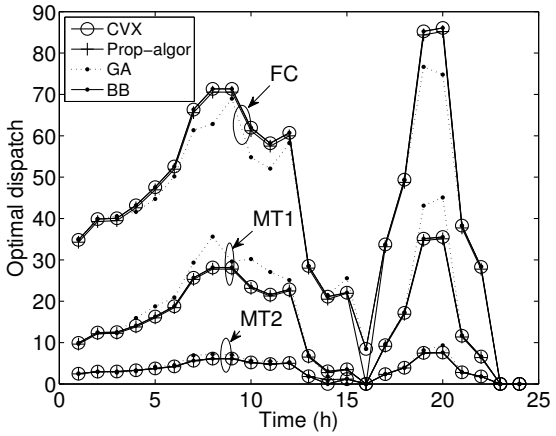


Figure 2.3: Performance comparison of different optimization algorithms for optimal dispatch of DGs under $PSS = 90\%$.

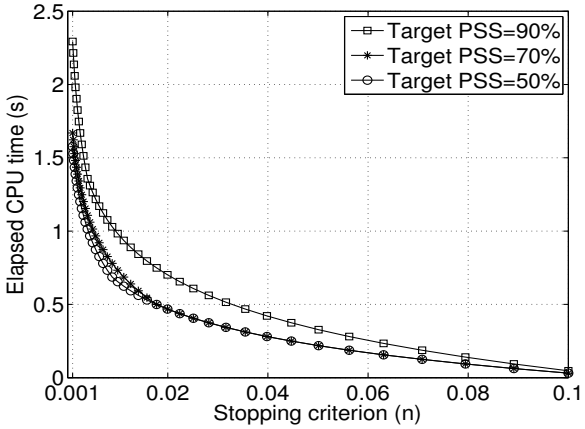


Figure 2.4: Elapsed CPU time of the subgradient-based algorithm under different stopping criterions.

Table 2.2: Unit Commitment of the Distributed Generators with Target $PSS = 70\%$

| **Unit** | **Hours (1-24)** |
|---|---|
| MT1 | 1 1 1 1 1 1 1 1 1 1 1 1 1 0 0 0 1 1 1 1 1 0 0 0 |
| MT2 | 1 1 1 1 1 1 1 1 1 1 1 1 0 0 0 0 1 1 1 1 1 0 0 0 |
| FC | 1 1 1 1 1 1 1 1 1 1 1 1 1 1 1 0 1 1 1 1 1 1 0 0 |

operational cost characteristics as well as emissions.

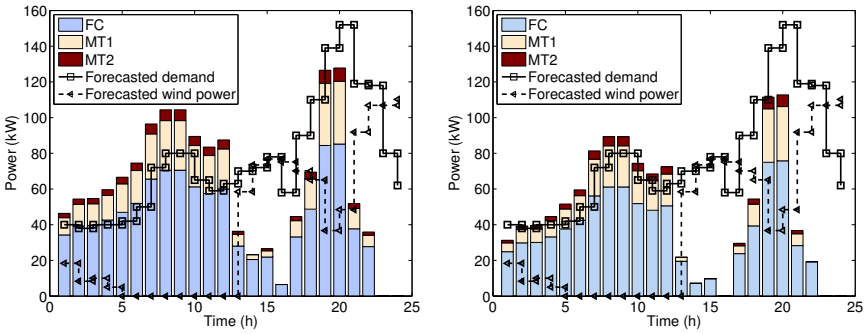


(a) Target $PSS = 90\%$ (b) Target $PSS = 70\%$

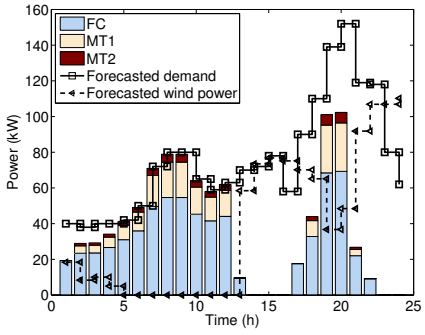


(c) Target $PSS = 50\%$

Figure 2.5: Forecasted demand and wind power, as well as optimal dispatch of the DGs under different PSS targets.

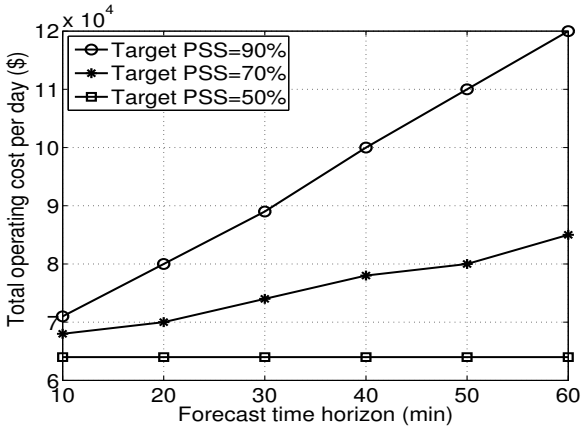


Figure 2.6: Total operating cost per day under different time horizons.

### 2.4.2 Operating Cost versus Different Forecasting Time Horizons

Clearly, the shorter the forecasting interval is, the more accurate the forecast data and the smaller the variance of the forecast error. According to [27], the typical standard deviation

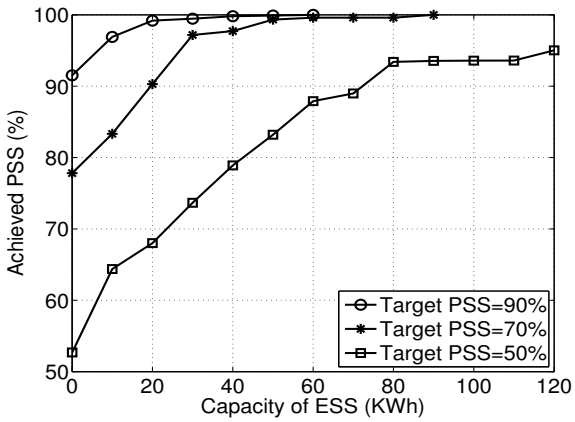


Figure 2.7: Achieved PSS versus the capacity of the ESS based on wind power statistics collected in one month.

of the wind power forecast error for a specific wind farm can be expressed as a function of the forecast horizon, which can be approximated accurately by a linear function when the forecast horizon is less than 6 hours. Fig. 2.6 examines the impact of varied forecasting time horizons on the total operating cost, based on the afore-mentioned linear model. Observe that for the case of $PSS = 90\%$, the operating cost grows almost linearly as the forecasting interval increases from 10 minutes to 1 hour. The same trend is observed for the case of $PSS = 70\%$. Interestingly, the cost holds constant for the case of $PSS = 50\%$, due to the fact that the microgrid is indifferent to either being connected to, or autonomous of the macrogrid.

### 2.4.3 The Impact of ESS on Microgrid's Autonomy

In the last numerical example, we incorporate the ESS into the microgrid setting and study the impact of the ESS on the achieved level of autonomy of the microgrid. To verify the effectiveness of the ESS on the achieved PSS, data samples collected by the Wind Test Center [31] in one month are employed to calculate the achieved PSS of the microgrid in practice. We observe from Fig. 2.7 that for all the PSS targets, 1) the proposed approach successfully meets the design targets in the absence of the ESS. For example, the microgrid achieves a

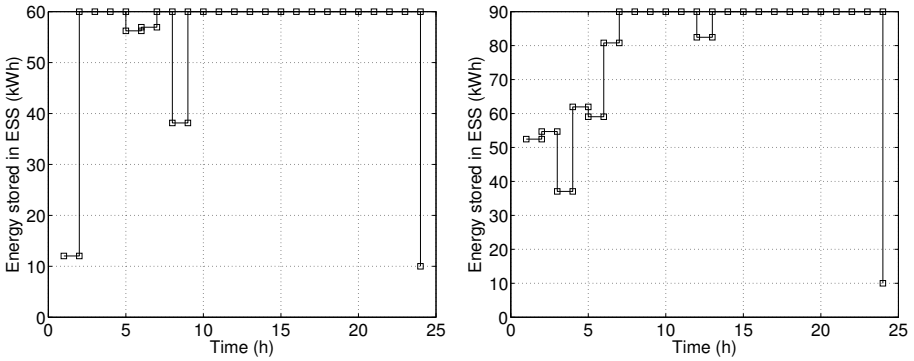


(a) Target $PSS = 90\%$




(b) Target $PSS = 70\%$

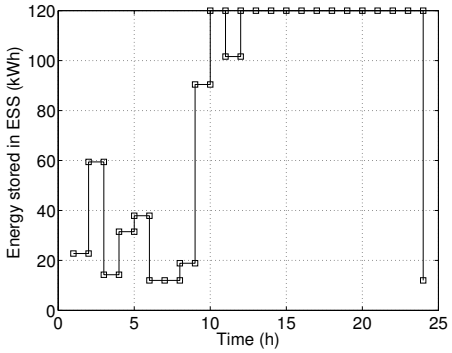


(c) Target $PSS = 50\%$

Figure 2.8: Variations in the amount of energy stored in ESS in one day under different PSS targets.

practical PSS of 52%, 78%, and 92% when the PSS targets are set as 50%, 70%, and 90%, respectively; 2) the microgrid is more capable of functioning self-sufficiently as the capacity of the ESS increases; 3) the achieved PSS hits an upper limit when the capacity of the ESS is larger than a threshold. From our simulations, this ESS threshold grows from 40 kWh, to 90 kWh, and to 120 kWh as the PSS targets decreases from 90% to 70%, and to 50%. This provides a guideline on determining the ESS size to achieve a desired PSS level.

To further analyze the variations of the energy stored in the ESS in one day, we plot in Fig. 2.8 the evolution of the energy stored in ESS under different target PSSs. The capacity of ESS is set as 60 kWh, 90 kWh, and 120 kWh as in Fig. 2.8(a), Fig. 2.8(b), Fig. 2.8(c) when the PSS targets equal 90%, 70%, and 50%, respectively. Due to practical concerns, the

starting ($t = 0$) and ending limits ($t = 24$) of the ESS in this work are set as around 10% of the capacity of the ESS, which are 10 kWh for all the cases. We then observe that the events of charging and discharging occur frequently during the time period between 0:00 am to 10:00 am, when the forecasted wind power falls short of the forecasted demand. Note also that the stored energy in the ESS varies less remarkably as the microgrid tends to operate more independently.

## 2.5 Conclusion

The unique characteristics of renewable-powered microgrids have brought new challenges to the classic UC optimization task of unit commitment. We have shown that the traditional problem formulation can be modified to incorporate the intermittency of the RESs, emission limits on the carbon footprint, as well as forecast errors that exist in demand and renewable power forecasts. Using a duality-based approach, it has been demonstrated that an analytical characterization of the optimal commitment and dispatch solutions for the distributed generators is available, which can be computed very efficiently using a subgradient-based algorithm. The approach can be easily modified to incorporate other types of distributed generators or RESs. Our work in this chapter shows that the features of DGs can have a great impact on the operation of UC strategy in microgrids, which will be investigated in our future work.

# Chapter 3

# Short-Term Operation Scheduling in Renewable-Powered Microgrids (Connected Mode)

In Chapter 2, we successfully find a method to determine the least-cost UC and the associated dispatch in a microgrid in the islanded mode. In this chapter, we further study the UC problem when the microgrid has the interaction with the main grid, a typical connected mode. The role of the macrogrid is also changed to both producer and consumer in this new grid framework, which is an extended situation built upon the second market policy. The problem formulation is revised and the solving procedure is also modified to incorporate the interconnection with the main grid.

## 3.1 Introduction and Motivation

The microgrid as a novel concept has been proposed, discussed and practiced in the power system academia for over 10 years, and the Smart Grid paradigm has attracted an unprecedented level of industrial and political support globally, which grants microgrid a promising

chance of imminent commercialization. From the perspective of microgrid, one of the most salient benefits is that it possesses the ability of switching to the islanded mode either if the main grid (i.e., macrogrid) faults or the real time price of energy from the macrogrid is much higher compared to the local generation. On the other hand, the encouragement of utilizing more renewable energy sources might produce surplus energy in the microgrid which can be sold to the macrogrid for more profit. The realization of this ideal interaction between microgrid and macrogrid is based upon the real time two-way communication and the advanced controlling schemes in the system. The role of the macrogrid is also changed from only a producer to both producer and consumer in the future grid framework. This adaptation would help to relieve the pressure of power demand in the peak load time, reduce the energy waste, and at the same time, cut down the operation cost of a microgrid effectively.

In the previous chapter, we only focused on the UC and dispatching problem when a microgrid is in the "island mode". Whereas in this chapter, the interaction with the main grid will be in consideration for a complete study. As an extension of the UC scheduling problem in "island mode", a typical "connected mode" with the proposed hierarchical control architecture is shown in Fig. 3.1, with the following control levels: [6, 32, 33]:

- distribution management system (DMS);
- microgrid system central controller (MGCC);
- local microsource controllers (MC) and load controllers (LC).

The MC utilizes the power electronic interface of the DG, tracks the local information (i.e., environment and capacity) and controls the voltage and the frequency of the microgrid following the demands from the central controller. The LC is installed at the controllable load and reports the demand requests following the orders from the MGCC for load management. The MGCC is responsible for the optimal operation considering the market prices of

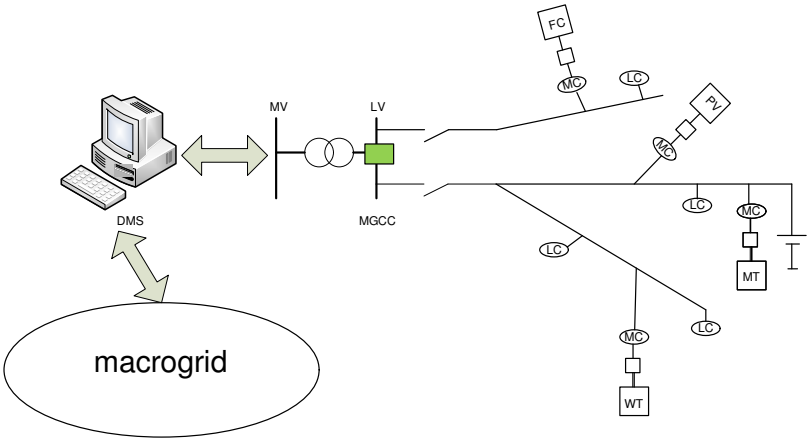


Figure 3.1: Microgrid Structure

electricity from the distribution system as well as local production capabilities. The issues of islanded or interconnected operation of the microgrids and the related exchange of information with the MGCC are taken care of by the DMS. The UC and dispatching problems of the microgrid in both operational modes are processed in the MGCC given the price of trading information, local capacity and demand requests from the DMS, MC, and LC, respectively. The optimization procedure depends on the market policy adopted in the operation. In this work, the following two classical operation policies are described:

1. The microgrid is separated from the upstream distribution grid and aims at minimizing the operational cost while satisfying the total demand or the critical demand that relate to essential processes that must always be powered to guarantee reliability to some extent.

2. The microgrid participates in the open market, purchasing/selling power from/to the macrogrid to reduce the operational cost and at the same time, fulfills the total demands in the local size.

In the first policy, the MGCC aims to fulfill a fixed reliability of the microgrid, using its local generation without absorbing power from the upstream grid. Mathematically, the MGCC minimizes the operational cost, taking into account the constraints of environmental

requirements and probability of self-sufficiency. This is the main problem we dealt with in Chapter 2, upon which the new extended situation is built upon with the second market policy.

The remainder of this chapter is organized as follows. Section 3.2 discusses the basic system models with the interactions with the main grid. Next, in Section 3.3, the optimal service restoration problem is formulated and finally solved with some technical adjustments. Section 3.4 conducts numerical simulations that verify the feasibility of the proposed scheme. Finally, concluding remarks are drawn in Section 3.5.

Table 3.1: Nomenclature of Chapter 3

| Symbol | Description |
|---|---|
| $\alpha,\ \beta$ | Load priority constants |
| $b_b,\ b_s$ | Purchasing and selling price from and to the main grid |
| $t$ | Time instance |
| $u_{b,t},\ u_{s,t}$ | Status indicator of purchasing, selling energy with the main grid |
| $C_t(E_t)$ | Cost of selling energy to the main grid, ($\leq 0$) meaning the profit |
| $C_t(I_t)$ | Cost of purchasing energy from the main grid |
| $Cons$ | Constant value in the Lagrangian function |
| $D_{top,t}$ | Critical demands at $t$ |
| $E^{max},\ I^{max}$ | Purchasing and selling bounds with main grid in one time instance |
| $E_t\ I_t$ | The amount of electricity in the trading at one time instance $t$ |
| $K$ | The number of DGs |

## 3.2 System Models

We also consider a microgrid that consists of a set of $N$ DG units, MTs, FCs, and WTs, however, in this chapter, the main grid is another power source as well as a consumer. As a result, the system models are different from the previous models in Chapter 2. The electrical loads in the microgrid are prioritized into two tiers too, critical loads and non-critical loads, and in our work the former one should be fulfilled by the local generations with some probability. We assume the microgrid schedules its units to meet the local loads in the highest priority, satisfy the non-critical loads using best efforts, and at the same time purchase power from the main grid in case of supply shortage. If the power generated from the local sources is larger than the local demands, the selling transaction with the main grid is considered. Besides, the microgrid updates the UC strategy every one hour, during which load, generation, and the price of power purchasing/selling from/to the main grid are considered constant. Except for the models mentioned below, others can refer to Chapter 2. Parameters are listed in the Nomenclature in Table 3.1.

### 3.2.1 Cost Models for Transactions with Main Grid

Compared to the quadratic operating cost of an MT/FC, the cost of merchandise with the main grid is assumed linear in our work.

**Purchasing Costs.** The power cost purchased from the main grid can be considered as a linear model, which can be expressed as,

$$C_t(I_t) = b_b \cdot I_t, \tag{3.1}$$

$$0 \leq I_t \leq I_{max}. \tag{3.2}$$

**Selling Costs.** The power profit selling to the main grid is also a linear model,

$$C_t(E_t) = b_s \cdot E_t, \tag{3.3}$$

$$E_{max} \leq E_t \leq 0. \tag{3.4}$$

### 3.2.2 Emission Models

Emission effects should be taken into account for environmental friendly power production. Generally speaking, the amount of emissions produced depends on fuel used, pollution control devices installed, and the amount of electricity generated. In this work, we assume that DGs and the power purchased from the main grid produce emissions, and the RESs are emission-free. Besides, the emissions of the power sold to the main grid are not considered in the microgrid side. As in Chapter 2, a quadratic function is also considered as follows,

$$\sum_{i=1}^{K}(\alpha_i p_{i,t}^2 + \beta_i p_{i,t} + \gamma_i) + (\alpha I_t^2 + \beta I_t + \gamma). \tag{3.5}$$

### 3.2.3 Probability of Self-sufficiency

Similar to the PSS in Chapter 2, both demands and renewable power forecast are prone to errors, and once a microgrid cannot meet power demand solely based on local generating units, it can switch to a connect mode and purchase energy from the main grid. However, we assume in this work that the critical demands should be met by the microgrid energy supply with some probability. As a result, the probability of self-sufficiency can be reformulated as

$$P\left(\sum_{i=1}^{N} p_{i,t}u_{i,t} + \widehat{p}_{w,t} + \Delta_w \geq D_{top,t} + \Delta_d\right) \geq PSS. \tag{3.6}$$

### 3.2.4 Power Balance

The power balance within the MG should be given careful attention, and satisfaction of all local demands is critical for the system reliability.

$$\sum_{i=1}^{K} p_{i,t}u_{i,t} + \widehat{p}_{w,t} + I_t \cdot u_{b,t} + E_t \cdot u_{s,t} = D_t. \tag{3.7}$$

## 3.3 Problem Formulation and Solutions

Based upon the aforementioned cost models and system constraints, we formulate the UC optimization problem which is to determine the loads and commitments of DGs and power exchange with the main grid. Then a duality-based analysis is used to derive the closed-form solutions.

### 3.3.1 Problem Formulation

Similar to problem **P1** in Chapter 2, we now formulate problem $\mathbf{P_{connect}}$ including the interaction with the main grid,

$$
\begin{aligned}
\mathbf{P_{connect}} \quad \min_{\substack{p,I,E,u \\ \forall i=1,\dots,K}} \quad & \sum_{i=1}^{K}(a_i p_{i,t}^2 + b_i p_{i,t} + c_{i,t})u_{i,t} + b_b \cdot I_t \cdot u_{b,t} + b_s \cdot E_t \cdot u_{s,t} \\
\text{s.t.} \quad & P\left(\sum_{i=1}^{K} p_{i,t}u_{i,t} + \widehat{p}_{w,t} + \Delta_w \geq D_{top,t} + \Delta_d\right) \geq PSS && (3.8) \\
& \sum_{i=1}^{K}(\alpha_i p_{i,t}^2 + \beta_i p_{i,t} + \gamma_i)u_{i,t} + (\alpha I_t^2 + \beta I_t + \gamma)u_{b,t} \leq \zeta && (3.9) \\
& \sum_{i=1}^{K}(p_i^{max} - p_{i,t}u_{i,t}) \geq R_t && (3.10) \\
& \sum_{i=1}^{K} p_{i,t}u_{i,t} + \widehat{p}_{w,t} + I_t \cdot u_{b,t} + E_t \cdot u_{s,t} = D_t && (3.11) \\
& E^{max} \leq E_t \leq 0 && (3.12) \\
& 0 \leq I_t \leq I^{max} && (3.13) \\
& p_i^{min} \leq p_{i,t} \leq p_i^{max}, \ \forall i = 1, ..., K && (3.14)
\end{aligned}
$$

$b_b$ and $b_s$ are the purchasing and selling prices with the macrogrid, respectively, and are assumed to be provided by the open market with the condition $b_b > b_s$. Other parameters are all in the Nomenclature of Table 2.1.

It can be figured out that $\mathbf{P_{connect}}$ is also a mixed-integer UC problem with a nonlinear solution space. The objective is to minimize the operation cost including the interaction with the main grid, and at the same time fulfill the total demands in (3.11). Electrical loads in the microgrid can be prioritized into tiers, and self-sufficiency is still a reliability index in the connect mode. Therefore, the constraint (3.8) is kept in the new problem to reflect the autonomy on *critical loads* in the microgrid. Besides, to limit the greenhouse gas emissions, (3.9) is included in the constraints. We solve this mixed-integer programming problem with

convex transformation, variables decomposition, and the Lagrangian relaxation similar to **P1** in Chapter 2. There are some adjustments in the solving procedures depending on the new features.

After the convex transformation and variable decomposition, we have the Lagrangian function written as,

$$\mathcal{L}(\lambda_t, \mu_t, \nu_t, g_t, \mathbf{p}, \mathbf{u}, I_t, E_t) = \sum_{i=1}^{K} u_{i,t}\varphi_{i,t}(p_{i,t}) + u_{t,b}\varphi_{I,t}(I_t, \mu_t) + u_{t,s}\varphi_{E,t}(E_t, g_t) + Cons, \quad (3.15)$$

where $\varphi_{i,t}(p_{i,t})$, $\varphi_{I,t}(I_t, \mu_t)$ and $\varphi_{E,t}(E_t, g_t)$ are viewed as the indication functions

$$\varphi_{i,t}(p_{i,t}) = (a_i + \mu_t\alpha_i)p_{i,t}^2 + (b_i + \mu_t\beta_i - \lambda_t + \nu_t - g_t)p_{i,t} + c_i + \mu_t\gamma_i, \quad (3.16)$$

$$\varphi_{I,t}(I_t, \mu_t) = (\mu_t\alpha)I_t^2 + (b_b + \mu_t\beta - g_t)I_t + \mu_t\gamma_t, \quad (3.17)$$

$$\varphi_{E,t}(E_t, g_t) = (b_s - g_t)E_t. \quad (3.18)$$

Then the form of the solutions is based on the value of the Lagrangian multiplier $\mu_t$:
If $\mu_t \neq 0$,

$$p_{i,t}^* = \underset{p_i^{min} \le p_{i,t} \le p_i^{max}}{\arg\min} \varphi_{i,t}(p_{i,t}) = \left[ -\frac{b_i + \mu_t\beta_i - \lambda_t + \nu_t - g_t}{2(a_i + \mu_t\alpha_i)} \right]_{p_i^{min}}^{p_i^{max}} \quad (3.19)$$

$$I_t^* = \arg\min \varphi_{I,t}(I_t) = \left[ -\frac{b_b + \mu_t\beta - g_t}{2(\mu_t\alpha)} \right]_0^{I^{max}} \quad (3.20)$$

$$E_t^* = \arg\min \varphi_{E,t}(E_t) = \begin{cases} E^{max} & b_s - g_t > 0 \\ 0 & b_s - g_t < 0. \end{cases} \quad (3.21)$$

$$u_{i,t}^*(\text{or } u_{b,t}^*, \text{or } u_{s,t}^*) = \begin{cases} 1 & \varphi_{i,t}(p_{i,t}^*) < 0 \text{ (or } \varphi_{I,t}(I_t^*) < 0, \text{or } \varphi_{E,t}(E_t^*) < 0), \\ 0 & \text{Otherwise.} \end{cases} \quad (3.22)$$

If $\mu_t = 0$, and $|b_b - g_t| \leq 0.05$, the power to buy from the main grid should be adjusted as,

$$I_t^* = [D_t - (\sum_{i=1}^{K} p_{i,t} u_{i,t} + \widehat{p}_t)]_0^{I^{max}}, \tag{3.23}$$

$$u_{b,t}^* = 1. \tag{3.24}$$

If $\mu_t = 0$, and $|b_s - g_t| \leq 0.05$, the power to sell to the main grid should be adjusted as,

$$E_t^* = [D_t - (\sum_{i=1}^{K} p_{i,t} u_{i,t} + \widehat{p}_t)]_{E^{max}}^0, \tag{3.25}$$

$$u_{s,t}^* = 1. \tag{3.26}$$

So far, we have found the analytical optimal solutions, which are functions of the Lagrangian multipliers. By convexity, it suffices to obtain the optimal dual variables $(\lambda_t^*, \mu_t^*, \nu_t^*, g_t^*)$ to the dual problem with the key iteration steps:

$$\lambda_t^{(n+1)} = \left[\lambda_t^{(n)} + \tau^{(n)} \left(A_t - \sum_{i=1}^{K} u_{i,t}^{*(n)} p_{i,t}^{*(n)}\right)\right]^+, \tag{3.27}$$

$$\mu_t^{(n+1)} = \left[\mu_t^{(n)} + \tau^{(n)} \left(\sum_{i=1}^{K} (\alpha_i p_{i,t}^2 + \beta_i p_{i,t} + \gamma_i) u_{i,t} + (\alpha I_t^2 + \beta I_t + \gamma) u_{b,t} - \zeta\right)\right]^+, \tag{3.28}$$

$$\nu_t^{(n+1)} = \left[\nu_t^{(n)} + \tau^{(n)} \left(R_t - \sum_{i=1}^{K} \left(p_i^{max} - p_{i,t}^{*(n)} u_{i,t}^{*(n)}\right)\right)\right]^+, \tag{3.29}$$

$$g_t^{(n+1)} = \left[g_t^{(n)} + \tau^{(n)} \left(D_t - \widehat{p}_{w,t} - \left(\sum_{i=1}^{K} u_{i,t}^{*(n)} p_{i,t}^{*(n)} + I_t \cdot u_{b,t} + E_t \cdot u_{s,t}\right)\right)\right]^+. \tag{3.30}$$

## 3.4 Numerical Simulations and Discussion

In this section, a microgrid consists of one MT, one FC, one WT and exchanges energy with the main grid if the generation is not sufficient or exceeds the local demands. The scheduling time horizon is still 24 hours. The fuel cost coefficients, the emissions coefficients, and the

Table 3.2: Parameters of Distributed Generators

| **Unit** | $a_{(.)}$(\$/kW$^2$) | $b_{(.)}$(\$/kW) | $c_{(.)}$(\$) | $\alpha_{(.)}$(kg/kW$^2$) | $\beta_{(.)}$(kg/kW) | $\gamma_{(.)}$(kg) | $p_{(.)}^{max}$ |
|---|---|---|---|---|---|---|---|
| MT | 1 | 50 | 10 | 3.49 | $-5.554$ | 4.091 | 400 kW |
| FC | 5 | 20 | 2 | 1.38 | $-3.551$ | 5.326 | 400 kW |
| I | $\times$ | $\times$ | $\times$ | 4.25 | $-3.551$ | 5.326 | 300 kW |
| | | | | $\times 10^{-4}$ | $\times 10^{-4}$ | $\times 10^{-4}$ | |

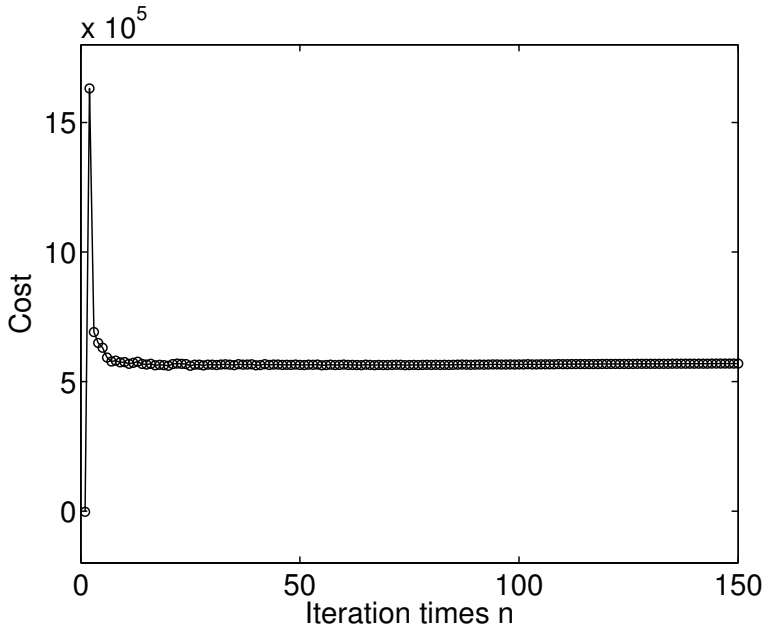


Figure 3.2: Operation Cost in Connect Mode, $PSS = 90\%$

power limits of DGs are listed in Table 3.2. The price of purchasing $b_b$ and selling $b_s$ are set to be 2 and 1.8 dollars/$kW$, respectively, and the maximum amount of power that can be sold to the main grid at $t$ is $-100$ kW. Other parameters are set the same as in Chapter 2. The simulation shall illustrate the derived unit commitment solutions for the connect mode without considering the functionality of the ESS. Fig. 3.2 illustrates the fast convergence behavior of the proposed algorithm in optimizing the total operating cost with $PSS = 90\%$. The optimal amount of dispatch of each DG for given demand and wind power forecast profiles are shown in Fig. 3.3. Fig. 3.3(a) provides us both the critical demands and whole local demand, and the former one should be satisfied by the DGs under a probability of

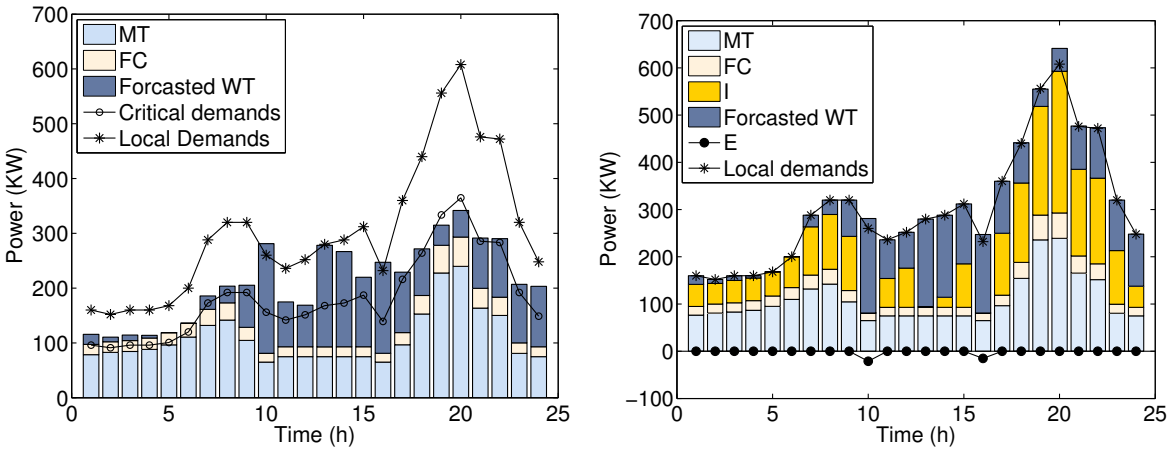


(a) Without power exchange with main grid

(b) With power exchange

Figure 3.3: Optimal dispatch of the DGs as well as the power exchange with the main grid, $PSS = 90\%$.

$PSS = 90\%$. Observing the differences between the critical demands and the generations, the insufficiency takes place at 19:00 pm to 20:00 pm, and the excesses at other times will be provided to the non-critical demands. During the entire process in Fig. 3.3(b), the reliability of the whole system is improved through the power exchange with the main grid. Especially at 10:00 am and 16:00 pm, the excess energy generated from the MG can be sold to the main grid at the price of $b_s$.

## 3.5 Conclusion

In this Chapter, it is shown that the method proposed in Chapter 2 can be modified to incorporate the interconnection with the main grid, considering the emission limits and intermittency of RESs. Using the duality-based approach, it has been demonstrated that the new problem is also convex and the analytical solutions of the optimal commitment and dispatch for the distributed power sources are available, which also efficiently improves the reliability of the MG system.

# Chapter 4

# Service Restoration for a Renewable-Powered Microgrid in Unscheduled Island Mode

From the perspective of the microgrid, one of the most salient benefits is switching to the islanded mode either if the real time price of energy from the macrogrid is much higher than the local generation or the main grid faults. The former situation is considered in the previous chapters, and in this chapter we will study the latter case. A microgrid should be connected with the main grid most of the time. However, when a blackout of the main grid happens, especially an unscheduled breakdown, the microgrid needs to be automatically sectionalized and fulfill the local demands as fast as possible. We propose two scenario-splitting methods to efficiently solve this service restoration problem with uncertainties.

## 4.1 Introduction and Motivation

In recent years, a number of technical, cost, and societal factors came together to drive the microgrid (MG) as one of the biggest changes in the electric power infrastructure on the

horizon. Moreover, the growing penetration of renewables and other generation technologies, e.g., inverter-based small scale wind, solar photovoltaics (PV) and clean diesel, have propelled the development of the MG [34]. The term *microgrid*, sometimes referred to as *distributed resources (DR) island systems*, is used for some intentional islands [35]. An MG has the ability to disconnect from and parallel with the main grid so as to operate in both the "island mode" or "grid-connected". The interconnection with the main grid is being addressed via numerous pilot projects [36].

A transition to island mode can be triggered by a *scheduled* or *unscheduled* event [35],[37], and the latter is the situation considered in our work, which is an inadvertent event initiated by fault or loss of connection to the main grid. In practice, normal operations are often disrupted by sudden breakdowns and their durations are not certain but stochastic. So this situation is much more practical and challenging. In this case, the DR system needs to be automatically sectionalized through control and protection procedures, and a load management strategy is also needed in the MG blackstart operation. This can be seen as a service restoration (SR) problem which is a traditionally critical topic in distribution engineering [38]. The whole restoration is usually simpler for an island MG due to the reduced number of controllable variables, i.e., loads and switches. On the other hand, if there are multiple DR units in the system, the control operation should be scheduled and coordinated to efficiently fulfill the needs of the local island, while guaranteeing the system frequency and voltage requirements [39],[40] usually through $DC/AC$ or $AC/DC/AC$ power electronic inverters of the DRs [41]. Besides, the whole operation requires communication and interaction among DRs and the controlling center, and the updated information should be monitored before disconnection, such as the demands, generation, and the status of the current switches at the time of breakdown, probability of each breakdown scenario, etc. Detailed MG controlling architectures and the assumed sequence of actions for MG blackstarts can be referred to [41, 42, 43, 44].

Considerable efforts have been placed on the analysis and methods to improve the SR plans. To achieve the restorative tasks effectively, several knowledge-based approaches have been suggested, including the expert systems [45] and artificial neural networks [46]. However, these methods only provide a reasonable numerical solution (suboptimal) and have high computational complexity. Later some optimization methods are proposed, such as branch and bound techniques combined with the interior points linear programming [47], and dynamic programming with state reduction [48]. These techniques can lead to optimal solutions but the procedure is not efficient unless large portions of the solution space can be quickly discarded when there are not too many solutions having near optimal objective values. Furthermore, most of these works consider only the deterministic SR problem, which is much simpler and saves a lot of computation and complexity. The classic progressive hedging method [49] is often used to deal with general stochastic problems but it may not converge in the SR problem with uncertain breakdown time, which involves integer decision variables.

This work deals with the SR multi-stage scheduling problem in an island MG system with multiple DR units consisting of a radial configuration and provides two stochastic methods to solve it. The contributions of the work are as follows: 1) in light of the requirements of controlling procedures of an MG and to take into account two types of uncertainties, i.e., the duration of disconnection and the forecasted renewable power generations, a stochastic integer problem formulation is proposed; 2) the optimization problem is solved in an efficient two-step procedure with less computation and complexity, compared to the classic progressive hedging (PH) algorithm, which is a scenario-based decomposition technique for solving stochastic programs. The comparison demonstrates the advantages of our proposed methods in terms of efficiency and accuracy; 3) the proposed methods provide guidelines to MG design, i.e., configuration of the power network, the suitable capacity of each DR unit including the energy storage systems (ESS), to increase the reliability of the local system.

The remainder of this Chapter is organized as follows. Section 4.2 discusses the basic system models including demands priority, general assumptions and constraints in the island operation, as well as uncertainties in the system. Next, in Section 4.3, the integer optimal service restoration problem is formulated and solved. Section 4.4 conducts numerical simulations that verify the accuracy and feasibility of the proposed scheme. Finally, concluding remarks are in Section 4.5. For the nomenclature in this chapter, please refer to Table 4.1.

Table 4.1: Nomenclature of Chapter 4

| Symbol | Description |
|---|---|
| $\alpha_{(.)}, \beta_{(.)}$ | Priority level of critical and non-critical loads |
| $\triangle_{(.,.)}$ | Synchronized ramping rate of one DR unit |
| $\varepsilon$ | Convergence criterion parameter |
| $\Delta_w$ | Wind power forecast error |
| $\varphi_{(.,.)}, \xi_{(.,.)}, \rho^{(.)}_{(.,.)}$ | Lagrangian multiplier |
| $\mu_w$ | Mean of wind power forecast error |
| $\sigma_w^2$ | Variance of wind power forecast error |
| $\Gamma(s')$ | Beginning instant that scenario $s$ does not share a bundle with scenario $s'$ |
| $\mathcal{L}^{(.)}(.)$ | Lagrangian function |
| $\tau^{()}$ | Step size of each iteration |
| $\mathfrak{T}$ | Limitation of the operation times |
| $c_{(.)}$ | Operation cost of each switch |
| | demand can be fulfilled partially |
| $h$ ($h'$) | State index |
| $i$ | Load point index (subscript) |
| $j$ | Distributed generator index (subscript) |
| $q$ | Specific bus in which the first or the second priority can be fulfilled partially |
| $s'$ | The previous scenario of scenario $s$ |
| $s$ | Scenario index for different disconnection durations |
| $t$ | Time index (half an hour) |
| $t_0$ | Initial time when the breakdown happens |
| $u^*_{(.,.)}$ | Optimal critical loads status indicator |

| | |
|---|---|
| $u^{(.)}_{(.,.)}$ | Critical loads status indicator where 1 means satisfied and 0 means shed |
| $v^{*}_{(.,.)}$ | Optimal Non-critical loads status indicator |
| $v^{(.)}_{(.,.)}$ | Non-critical loads status indicator where 1 means satisfied and 0 means shed |
| $w_r$ | Wind power capacity |
| $x^{h}_{(.,.)}$ | Switch status indicator of state $h$ where 1 means closed and 0 means open |
| $\mathbf{x}_{(h,.)}$ | State $h$ consists of different status of $K$ switches |
| $C(.)$ | Total cost of operation from one state to another |
| $CostM$ | Transfer matrix of operation cost in different states |
| $D(.)$ | Dual function |
| $DP$ | Dynamic programming |
| $DR$ | Distributed resource |
| $E_{(.,.)}$ | Critical loads in one load bus at one time instant |
| $\widetilde{E}^{*}_{h,t}$ | The actual critical loads in bus $h$ at one time instant |
| $ESS$ | Energy storage system |
| $FC$ | Fuel cell |
| $G_{(j.t)}$ | Generation amounts of distributed resource in time instant $t$ including the target generation of wind turbines when $j = w$ |
| $\overline{G}_j$ | Capacity of each distributed unit |
| $H$ | Total number of possible states in the power network |
| $J^{s}_{h,t}(.)$ | Return function for state $h$ of scenario $s$ to proceed DP |
| $\overline{J}$ | Probability-based expected matrix to proceed DP |
| $K$ | Total number of switches in the power network |
| $L(.,.)$ | Total weighted restored loads |

| | |
|---|---|
| $M$ | Total number of distributed units |
| $M_{left}$ | Remainder of the generation |
| $MT$ | Microturbine |
| $MG$ | Microgrid |
| $N$ | Total number of load bus |
| $NumM$ | Transfer matrix of operation times in different states |
| $PH$ | Progressive hedging algorithm |
| $P_{s(.)}$ | Probability of different cases of breakdown duration |
| $\widehat{P}_{w,t}$ | Forecasted wind power in time instant $t$ |
| $Q_{(.,.)}$ | Non-critical loads in one load bus at one time instant |
| $\widetilde{Q}^{*}_{h,t}$ | The actual non-critical loads in bus $h$ at one time instant |
| $S$ | Total number of scenarios in disconnection durations |
| $SR$ | Service restoration |
| $T$ | Total possible breakdown horizon |
| $TD$ | Time decoupled |
| $WPFR$ | Wind power forecasting reliability |
| $WT$ | Wind turbine |
| $Z_{(.)}$ | Restorative zone corresponding to the distributed unit |
| $Z_w$ | Restorative zone corresponding to the wind WT |

## 4.2 System Model

We consider the service restoration problem in a microgrid that consists of a set of $M$ DR units, including microturbines (MTs), fuel cells (FCs), wind turbines (WTs), and $N$ load buses. If a general blackout occurs, local DR capabilities in an MG can be exploited to feed local customers until the main grid is re-connected. Due to the operational constraints of DRs, the local demands might not be satisfied fully but prioritized. We assume that electrical demands in the microgrid are prioritized into two tiers, which consist of, e.g., *critical demands* related to essential processes that should be met first and lower-priority *non-critical demands* that can be temporarily removed until adequate power is available [50]. The DRs will cooperate with each other to meet as many demands as possible during the blackout. Furthermore, switching operation schemes are needed to complete the power network reconfiguration so as to improve the distribution among the loads [42]. In addition to dealing with the uncertain wind generations, the scheduling scheme to be designed needs to adapt to an unforeseen breakdown from the main grid. In this chapter, we use a scheduling interval of half an hour in the whole service restoration procedure[1], during which demands and generations are considered constant.

### 4.2.1 Demands Priority

If there is insufficient generation in the MG to cover the full demands, a load-shedding scheme needs to be developed [35]. In our work, we assume that each load bus will report the needed amount of *critical loads* $E_{i,t}$ and *non-critical loads* $Q_{i,t}$ during the breakdown horizon[2], with $\alpha_i$ and $\beta_i$ the priority levels of the $i$th load bus. The total weighted loads $L$

[1]Depending on different application requirements, smaller updating intervals can be selected [51]. In practice, half an hour is meticulous for the wind power forecasting in most of the regions.

[2]We assume that the estimation of the demands on each load bus is reported accurately. And we could add other priority levels to the demands priority model. Here we just take two priority levels as an example.

can be written as

$$L(u,v) = \sum_{t=t_0}^{T} \sum_{i=1}^{N} (\alpha_i E_{i,t} u_{i,t} + \beta_i Q_{i,t} v_{i,t}). \tag{4.1}$$

Besides, power balance within the MG island should be given careful attention [35],[52], and we divide the whole MG power network into different restorative zones $Z_j$ corresponding to each DR. Then we have

$$\sum_{i \in Z_j} (E_{i,t} u_{i,t} + Q_{i,t} v_{i,t}) \leq G_{j,t}. \tag{4.2}$$

### 4.2.2 General Assumptions and Islanded Operation

Under the assumption that a central control system and communication infrastructures are available for MG restoration, it is possible to produce an automatic controlling procedure after the blackout, such as identification of one or multiple suitable and stable voltage references in the MG system [41], grid synchronization [43, 44], etc. It is assumed that the information about the status of the power network, including the switch states, local demands and generations of DRs in the MG, are updated immediately after the disruption [44]. And assume that the power supply for the communication system in the whole system is unaffected by the unscheduled breakdown. According to [41],[43], all DR units and loads should be disconnected from the main grid at the beginning of the blackout for the stability of the system.

In order to avoid large frequency and voltage deviations, some electric utilities limit the load pick-up to 5% of the synchronized generation [35],[46],[48]. While considering the ramping rates of DRs, the constraint is expressed as

$$0 \leq G_{j,t+1} - G_{j,t} \leq \triangle_{j,t}, \tag{4.3}$$

besides, each DR has the capacity

$$G_{j,t} \leq \overline{G}_j. \tag{4.4}$$

Power network reconfiguration, which is the process of altering the topology structures by changing the open/closed status $x_{k,t}$ of the *sectionalizing* and *tie* switches[3] [53], is considered as a feasible method of service restoration [46],[54]. However, the operational cost and the number of switching operations in the reconfiguration should be limited to achieve the restoration goal in an economical way. Then we have the total cost $C_{h,h'}$ from $t$ to $t+1$

$$C_{h,h'} = \sum_{k=1}^{K} c_k |x_{k,t}^{h} - x_{k,t+1}^{h'}|, \ h, h' \in 1, ...H \tag{4.5}$$

and the operation time constraint

$$\sum_{k=1}^{K} (x_{k,t} \oplus x_{k,t+1}) \leq \mathfrak{T}, \tag{4.6}$$

where $\oplus$ denotes addition modulo 2. Moreover, the switch operations in the whole process should be guaranteed to restore the network into a radial structure [52],[55], which can be expressed as

$$\mathbf{x}_{h,t} \in \text{radial structure}. \tag{4.7}$$

[3]There are two types of switches in distribution systems: normally closed switches which connect line sections, and normally open switches on the tie-lines which connect two primary feeders or restorative zones.

### 4.2.3 Restorative Operation Cost and States of Network Configuration

In order to solve this restorative problem efficiently, we introduce the definition of *restorative operation cost* in our model, which is related to but different from [52],[55]. In our system model:

- Restorative operation cost is assigned to the switches needed to change status from open to closed and vice versa.

- The operation cost $c_k$ depends both on the distance between the load bus and the power source in the restorative zone $Z_j$ and the switch type, i.e., *sectionalizing* or *tie* switches. In practice, the operation cost of each switch decreases with the reduction of the distance from the power source. It corresponds to choosing the closer de-energized area first for the restoration, in which some critical facilities are usually located. The larger cost is often assigned to the *tie* switches, which are of the lower operation priority in the restorative procedure. The specific operation cost strategy can be formulated by the power network designers depending on different situations.

- Even in a small MG island, there are many different switch strategies, i.e., the states of network reconfiguration. However, only a small subset of them are qualified states not only conforming to the cost requirements but also the limitation of the operation times. In our work, we denote $H$ possible configuration states as the restorative strategies which meet the operation constraints, and then the operation cost as well as number of switch status changes can be preprocessed by $H \times H$ transfer matrices $CostM(\mathbf{x}_t, \mathbf{x}_{t+1})$ and $NumM(\mathbf{x}_t, \mathbf{x}_{t+1})$ from $t$ to $t+1$.

### 4.2.4 Uncertainties in the System

**Scenario Bundle Constraints.** Scenario analysis, originally proposed by Rockafellar and Wets [49], is a widely applicable method for introducing uncertainty into practical decision problems [56]. Typically, in such problems some of the data is uncertain, and the performance measure to be optimized is the expected value of some quantity. If it is possible to delay the decision until after the uncertainty is resolved, then we are in the environment of the "wait-and-see" problem and in this case, the optimization problem is deterministic. However, often one has to make a decision without knowing in advance which scenario will occur. In such a case, the optimization problem must consider all possible scenarios and choose values of the decision variables to optimize the objective function.

We investigate the multi-stage service restoration problem in an MG with the scenario analysis mentioned above. Although the duration of disconnecting from the main grid is uncertain, one optimal decision strategy, which takes into account all the possible scenarios incorporating future time stages, must be determined and executed for the current time stage. This leads to the scenario bundle constraint. The scenarios spanning different time stages can be expressed as a scenario tree structure [56, 57, 58] in Fig. 4.1.

Scenario Tree Notation: each leaf is connected to exactly one node at time $t \in T$, and each of these nodes represents a unique realization up to time $t$. Two scenarios whose leaves are both connected to the same node at time $t$ have the same realization up to time $t$. Consequently, in order for a solution to be implementable it must be true that if two scenarios are connected to the same node at $t$, the values of the optimal variables must be the same under both scenarios for $t' \leq t$. We represent this property as a constraint by partitioning all the scenarios at each time stage into different *scenario bundles*.

Our restoration scheduling procedure for each scenario $s$ begins immediately after the blackout $t_0$, and ends at the scheduling horizon of $T = t_0 + s - 1$. The longest possible disconnection duration is assumed to be known, i.e., the total number of scenarios $S$ is

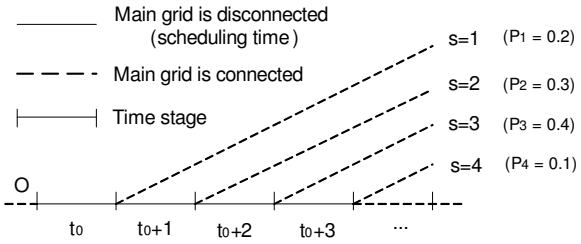


Figure 4.1: Scenario tree with 4 scenarios, $P_s = [0.2\ 0.3\ 0.4\ 0.1]$.

fixed. To better present the scenario bundle constraints, we define $\Gamma(s')$ as the first period in which the scenario $s$ does not share a bundle with the scenario $s'$. Then the constraints are expressed as [58],[59]

$$x^s_{k,t} = x^{s'}_{k,t}, \tag{4.8}$$

$$u^s_{i,t} = u^{s'}_{i,t}, \tag{4.9}$$

$$v^s_{i,t} = v^{s'}_{i,t}, \quad t = t_0, t_0+1, ..., \Gamma(s')-1. \tag{4.10}$$

**Reliability of Wind Power Forecasting.** Another uncertainty comes from the nature of the fluctuating wind production over big time scale. Wind power forecasts are prone to errors, which lead to difficulties to make accurate multi-stage restoration schedules in microgrid. As in [60], we propose a similar probability based concept, wind power forecasting reliability (WPFR), which indicates the target reliability that the wind generation forecasting can be achieved in the WT's restorative zone $Z_w$. We also assume that wind power forecast error $\Delta_w$ can be modeled as Gaussian distributed random variables [60, 27, 28], i.e., $\Delta_w \sim N(\mu_w, \sigma^2_w)$. Then the probabilistic power balance constraint for the wind power can be expressed as

$$P\left(\sum_{i\in Z_w}(E_{i,t}u_{i,t} + Q_{i,t}v_{i,t}) \le \widehat{p}_{w,t} + \Delta_w\right) \ge WPFR, \tag{4.11}$$

and is reformulated as

$$\sum_{i\in Z_w}(E_{i,t}u_{i,t}+Q_{i,t}v_{i,t}) \le \sqrt{2}\sigma_{w,t}\times erf^{-1}(1-2WPFR)+\widehat{P}_{w,t}+\mu_w = G_{w,t}. \tag{4.12}$$

## 4.3 Problem Formulation and Solutions

Based upon the aforementioned system models and operational requirements in an MG, and considering the uncertainties of both wind power forecasting generation and the unforeseen breakdown from the main grid, we formulate the optimization problem as problem **SR**[4]. The objective is to maximize the expected restored loads while minimizing the operational cost for a horizon of multiple time instants over $S$ possible scenarios.

$$\begin{aligned}\mathbf{SR}: \max_{u,v,x} \quad & \sum_{s=1}^{S}P_s\sum_{t=t_0}^{t_0+s-1}(\sum_{i=1}^{N}(\alpha_i E_{i,t}u_{i,t}^s+\beta_i Q_{i,t}v_{i,t}^s)-\sum_{k=1}^{K}c_k|x_{k,t}^s-x_{k,t+1}^s|)\\ \text{s.t.} \quad & (4.2),(4.3),(4.4),(4.6),(4.7),(4.8),(4.9),(4.10) \text{ and } (4.12).\end{aligned}$$

By observing the SR problem, we can find that in the objective function, the term $\sum_{i=1}^{N}(\alpha_i E_{i,t}u_{i,t}^s+\beta_i Q_{i,t}v_{i,t}^s)$ does not contain time coupled variables, while $\sum_{k=1}^{K}c_k|x_{k,t}^s-x_{k,t+1}^s|$ does. Similar observations can be made on the constraints. Hence we can decompose the problem into two steps. Step 1 optimizes ($\mathbf{u_t}$,$\mathbf{v_t}$) to achieve the maximum restored weighted loads by an efficient duality based subgradient method for a given network configuration, i.e., a set of $\mathbf{x_t}$, at a certain time stage. Step 2 calls dynamic programming to optimize the power network configurations, i.e., switch schemes $\mathbf{x_t}$, with the corresponding ($\mathbf{u_t}$,$\mathbf{v_t}$) from Step 1 to handle the time coupled problem. To deal with the scenario parameter $s$ and the scenario bundle constraints $(4.8)-(4.10)$, we propose two methods. The first method puts the probability $P_s$ into the return function of each state in every time stage of Step 2,

[4]Although the dimensions of $L(u,v)$ and $C(x)$ are different, the constant variables $\alpha,\beta$ and $\mathbf{c}$ can be designed to be the weight parameters depending on different applications.

using an average return function over all relevant scenarios for each time stage. The second method treats the SR problem in a sequential manner, without considering the probability of different disconnection scenarios. Based on the optimized decision variables for the previous time stage, the optimization is carried out for the current stage.

### 4.3.1 Method I: Expectation Solving Procedure

We first treat problem **SR** as $S$ independent sub-problems without considering the scenario bundle constraints. For each scenario $s$, the sub-problem is a linearly time-coupled integer problem, and a two-step solving procedure is given as follows.

**Step 1** : Based upon the explanation in Section 4.2.3, we have $H$ possible fixed network configuration states for the MG power system, and constraints (4.3), (4.4), (4.7) can be considered before the solving procedure. Step 1 treats the time-decoupled (TD) portion of the original SR formulation that

$$\begin{aligned} \textbf{TD}: \max_{u,v} \quad & \sum_{i=1}^{N}(\alpha_i E_{i,t} u_{i,t}^s + \beta_i Q_{i,t} v_{i,t}^s) \\ \text{s.t.} \quad & (4.2)(4.12). \end{aligned}$$

To solve this problem analytically, we use the Lagrangian relaxation technique with Lagrangian multiplier $\rho_{j,t}$

$$\mathcal{L}_t^s(\rho^{\mathbf{s}}, \mathbf{u}, \mathbf{v}) = \sum_{i=1}^{N} -(\alpha_i E_{i,t} u_{i,t}^s + \beta_i Q_{i,t} v_{i,t}^s) + \sum_{j=1}^{M} \rho_{j,t}^s (\sum_{i \in Z_j} (E_{i,t} u_{i,t}^s + Q_{i,t} v_{i,t}^s) - G_{j,t}). \quad (4.13)$$

We calculate the minimization of $\mathcal{L}_t^s$ with the initial arbitrary non-negative Lagrangian multiplier $\rho_{j,t}^s$ according to the following procedure:

The Lagrangian dual function is given by

$$D_t(\rho^s_{j,t}) = \min_{\substack{0\le u_{i,t}\le 1\\ 0\le v_{i,t}\le 1}} \mathcal{L}^s_t(\rho^s_{j,t}, \mathbf{u}, \mathbf{v}), \tag{4.14}$$

and the dual problem is

$$\max_{\rho^s_{j,t}\ge 0} D_t(\rho^s_{j,t}). \tag{4.15}$$

The dual function (4.14) is solved by minimizing (4.13) over ($\mathbf{u_t}$,$\mathbf{v_t}$). The minimum value is attained by setting $u^s_{i,t} = 1$ when the coefficient in front of $u^s_{i,t}$ is less than zero and $u^s_{i,t} = 0$ otherwise. This also applies to $v^s_{i,t}$.

$$(u^s_{i,t})^* = \begin{cases} 1 & \rho^s_{j,t} - \alpha_i < 0, \\ 0 & \text{otherwise.} \end{cases} \tag{4.16}$$

$$(v^s_{i,t})^* = \begin{cases} 1 & \rho^s_{j,t} - \beta_i < 0, \\ 0 & \text{otherwise.} \end{cases} \tag{4.17}$$

Then the subgradient method is used for solving the Lagrangian dual problem (4.15)

$$\rho^{(n+1),s}_{j,t} = \left[\rho^{(n),s}_{j,t} + \tau^{(n)} \left(\sum_{i\in Z_j} (E_{i,t}u^s_{i,t} + Q_{i,t}v^s_{i,t}) - G_{j,t}\right)\right]^+. \tag{4.18}$$

The iterations between (4.16),(4.17) and (4.18) lead to the optimal values ($\mathbf{u^*_t}$,$\mathbf{v^*_t}$) except for one element $u^s_{q,t}$ or $v^s_{q,t}$. When $\rho^s_{j,t} \ll \alpha_i$ or $\rho^s_{j,t} \gg \alpha_i$ of bus $i$, $u_i$ will quickly converge to $\{0, 1\}$. This applies similarly to $v_i$. However, because the generation may not be exactly divided in whole to the loads on buses, there is one bus, calling it $q$ with priority levels $\alpha_q$ and $\beta_q$, whose load is only satisfied partially. It is observed from the iteration process that

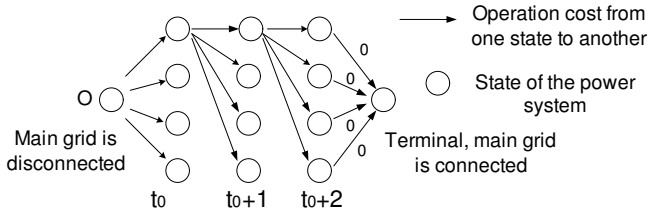


Figure 4.2: Dynamic Programming process with time stage 3, $H = 4$. The terminal state is added with zero operation costs.

$\rho_{j,t}$ will approach and fluctuate in the vicinity of $\alpha_q$ or $\beta_q$ of bus $q$ ($q \neq i$). Therefore, we make the following adjustment:

when $|\rho^s_{j,t} - \alpha_q| \leq \varepsilon$,

$$(u^s_{q,t})^* = 1, \tag{4.19}$$

$$\widetilde{E}^*_{q,t} = G_{j,t} - \sum_{i \in Z_j, i \neq q} (E_{i,t}(u^s_{i,t})^* + Q_{i,t}(v^s_{i,t})^*), \tag{4.20}$$

or when $|\rho^s_{j,t} - \beta_q| \leq \varepsilon$,

$$(v^s_{q,t})^* = 1, \tag{4.21}$$

$$\widetilde{Q}^*_{q,t} = G_{j,t} - \sum_{i \in Z_j, i \neq q} (E_{i,t}(u^s_{i,t})^* + Q_{i,t}(v^s_{i,t})^*). \tag{4.22}$$

This means the demand on load bus $q$ is only satisfied partially at the level of $\widetilde{E}^*_{q,t}$ or $\widetilde{Q}^*_{q,t}$. With this adjustment, all of the decision variables converge and it can be shown that problem **TD** is a relaxed integer linear problem, which is convex, and the duality gap between the primal problem and the dual problem is zero. A graphical convergence illustration can be found in Section 4.4.1.

**Step 2** : Given $\mathcal{D}_t(\rho^s_{j,t})$ of every state $h \in 1, ..., H$ at each time stage, we will solve the time-coupled sub problem for scenario $s$ with backward dynamic programming (DP) using

the **Bellman function** [61] given by

$$J^s_{h,t_0+s-1} = \mathcal{D}_{h,t_0+s-1}(\rho^s_{j,t_0+s-1}) + 0, \tag{4.23}$$

$$J^s_{h,t} = \min_{h' \in 1,...,H} \{\mathcal{D}_{h,t}(\rho^s_{j,t}) + C_{h,h'} + J^s_{h',t+1}\}. \tag{4.24}$$

With the initial value of $J^s_{h,t_0+s-1}(\mathbf{x}^s_{h,t_0+s-1})$ calculated from (4.23), for one stage $t$, $J^s_{h,t}(\mathbf{x}^s_{h,t})$, i.e., the return function, is obtained by minimizing the summation of the operation cost from $t$ to $t+1$ recorded in the transfer matrix $CostM(\mathbf{x}^s_t, \mathbf{x}^s_{t+1})$, $\mathcal{D}_{h,t}(\rho^s_{j,t})$ from Step 1, and $J^s_{h',t+1}$, as given by (4.24). This process continues for all the states over all time stages in scenario $s$. Fig. 4.2 illustrates the process of DP with 3 stages and 4 states.

In **Method I**, step 1 and step 2 are utilized to obtain the $H \times 1$ column vector $J^s_t$ with $t = t_0, ...t_0 + s - 1$ at every stage $t$ for each scenario $s$. To deal with the scenario bundle constraints (4.8)-(4.10), one probability-based expected matrix $\overline{J}$ with dimension $H \times S$ is created to indicate the average value of the return functions over all different scenarios. Each column of $\overline{J}$ is formulated as

$$\overline{J}_t = \sum_{s=1}^{S} P_s J^s_t \quad t = t_0, t_0 + 1, ..., t_0 + S - 1. \tag{4.25}$$

Then we find the solution $h$ of the shortest path at the current time stage, satisfying $\min_{h \in 1,...,H} \{\overline{J}_t + C_{h^*,h}\}$, with $h^*$ the network configuration solution of the previous time stage. Then the shortest path will be formed tracing forwardly from $t_0$ to $t_0 + S - 1$. The solution provided by **Method I** is sub-optimal with a small margin from the optimal results. However, the solving procedure is direct and efficient in practice.

### 4.3.2 Method II: Sequentially Solving Procedure

To solve Problem **SR** separately in different scenarios while considering the scenario bundle constraints (4.8)-(4.10), we treat the results of its previous scenario $s'$, i.e., $(s' = s-1)$ as the reference solutions for all time stages from $t_0$ to $t_0+s'-1$ and only need to solve the problem for the current time stage $t$. As a result, the solving procedure is sequential and the scenario bundle constraints are satisfied at the expense of some optimality. Similar to **Method I**, in Step 1 the analytical optimal solutions for each configuration state $h$ at each time stage $t$ is obtained through (4.14)-(4.22) based upon the pre-processed constraints (4.3), (4.4), (4.7). As for the optimal configuration state for operation in the current time stage, we choose $h'$ as the solution, satisfying $\min_{h'\in 1,\ldots,H}\{\mathcal{D}_{h,t}(\rho^s_{j,t}) + C_{h,h'}\}$ with the previous solution $h$ fixed as the reference. So far, we obtain the operation scheme sequentially, and note that for each scenario, only one stage optimization is needed, which is much less complex especially when the number of scenarios is large. Although the stochastic information $P_s$ has not played a role in this method, and the operational solution is sub-optimal for the original Problem **SR**, the solving procedure is efficient.

**Remark 1** − It is noticed that both of the proposed methods are sub-optimal. The reason for this is not the process of **Step 1**, which can provide us the optimal solution $(\mathbf{u}, \mathbf{v})$ for each time stage. The reason is due to the scenario bundle constraints resulting from the uncertainties of disconnection duration. The result of **Method I** is based on the expectation of all the scenarios, and provides a better solution when long durations of disconnection happen with higher probability. Oppositely, **Method II** outweighs **Method I** only if the probabilities of the short disconnection scenarios are larger.

Table 4.2: Configurations of power network with $H = 11$ state numbers (SNs), and 13 load buses are divided into 3 restorative zones (RZ).

| SN \ *RZ* | **MT** | **WT** | **FC** |
|---|---|---|---|
| 1 | 1,2,3,4 | 5,6,7,8,9 | 10,11,12,13 |
| 2 | 1,2,3,4 | 5,6,7,8,9,11 | 10,12,13 |
| 3 | 1,2,3,4 | 5,6,7,8 | 9,10,11,12,13 |
| 4 | 1,2,3,4,13 | 5,6,7,8,9 | 10,11,12 |
| 5 | 1,2,3 | 5,6,7,8,9 | 10,11,12,13 |
| 6 | 1,2,4 | 3,5,6,7,8,9 | 10,11,12,13 |
| 7 | 1,2,3,4,7 | 5,6,8,9 | 10,11,12,13 |
| 8 | 1,2,4 | 3,5,6,7,8,9,11 | 10,12,13 |
| 9 | 1,2 | 3,5,6,7,8,9 | 4,10,11,12,13 |
| 10 | 1,2,3,4,7 | 5,6,8 | 9,10,11,12,13 |
| 11 | 1,2,3,4,13 | 5,6,7,8,9,11 | 10,12 |

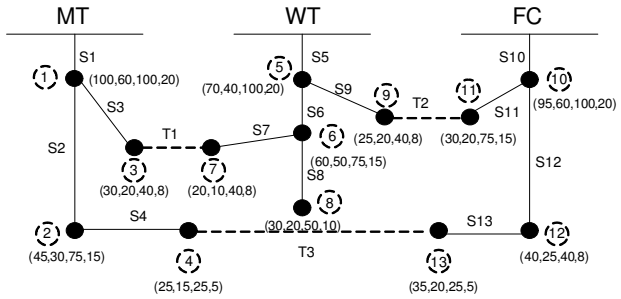


Figure 4.3: System network configuration of an island MG example with coefficients of demands and priority levels $(E_{i,t}, Q_{i,t}, \alpha_{i,t}, \beta_{i,t})$.

## 4.4 Simulation Results and Discussion

In this study, an island microgrid system consisting of one MT, one WT and one FC, is considered for a stochastic scheduling time horizon depending on the duration of the disconnection from the main grid. Our restoration strategy for the MG is further explained via an example system of Fig. 4.3, with the demands coefficients $E_{i,t}$, $Q_{i,t}$ kW and the priority level $\alpha_{i,t}$, $\beta_{i,t}$ of each load bus. The similar power network configuration has also been used in

[54],[62],[63]. Unless stated otherwise, we provide $H = 11$ candidate states for the power network configurations, i.e., different switch strategies, in Table 4.2. The state shown in Fig. 4.3 is assumed to be state 1, the state immediately after the disconnection occurs. As long as the candidate configuration states are set, both of the transfer matrices $CostM_{H\times H}(x_t, x_{t+1})$ and $NumM_{H\times H}(x_t, x_{t+1})$ can be obtained. The longest possible breakdown duration is 2 h, i.e., 4 time instants. We assume that any generations except wind power are all zero at the moment when the disconnection occurs without loss of generality, and the assumed synchronized generations from the MT and FC are $(100, 150, 250, 400)$ kW and $(100, 150, 300, 300)$ kW in 4 time instants, respectively. The wind speed data samples adopted in the work are from the "Cairngorm Automatic Weather Station" in the Heriot-Watt University Physics Department [64] with the parameters $v_{in} = 3.5$ m/s, $v_r = 14$ m/s, $v_{out} = 25$ m/s, $w_r = 400$ kW in the wind power estimation model of [60]. $v_{in}$, $v_{out}$, $v_r$ and $w_r$ are cut-in, cut-out, rated wind speed, and wind power capacity for the wind power estimation, respectively.

### 4.4.1 Restoration Schemes and Solution Convergence

This subsection illustrates the derived service restoration solutions mainly from the analysis of convergence and the duality gap. The probabilities of different cases $P_s$ are set to be $[0.1, 0.4, 0.3, 0.2]$. Clearly, the longer the forecasting interval is, the less accurate the forecasted data and the bigger the variance of the forecasted error, $\sigma^2_{w,t}$. According to [27],[60], the typical standard deviation, $\sigma_{w,t}$, of the wind power forecast error can be expressed as an approximated linear function of the forecast horizon when the forecast horizon is less than 6 hours. Thus the parameters are set as $\sigma_{w,t} = [1, 2, 3, 4]$, $\mu_w = 0$, and WPFR= 90%. The evolution of the subgradient-based algorithm in **Method II** is illustrated in Fig. 4.4. All of the four stages approach convergence after about 25 iterations, which also corresponds to the zero approaching duality gap witnessed in Fig. 4.4(b). This example verifies the proposed algorithm and provides us the optimal solution effectively within each time stage. To give

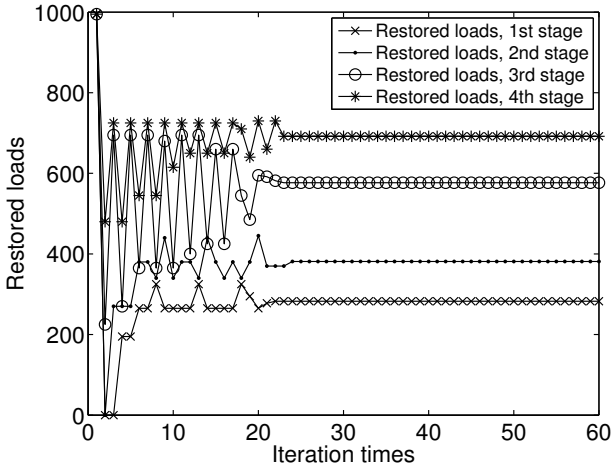


(a) Evolutions of the restored loads

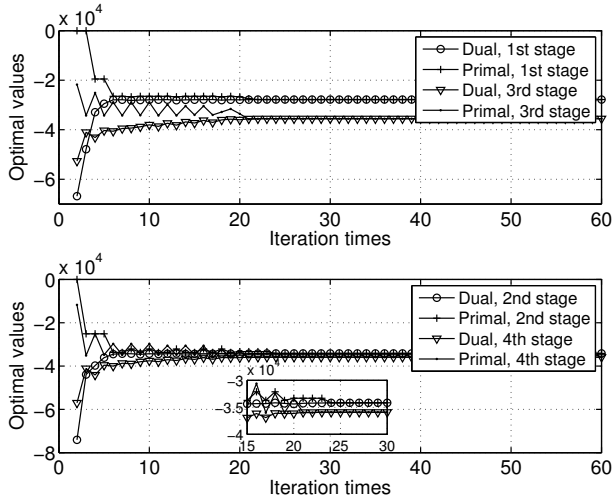


(b) Evolutions of the duality gap.

Figure 4.4: Evolutions of the optimal results.

more insight on the restoration scheduling scheme with priorities, we provide a stage-by-stage restoration process in two tiers in Fig. 4.5 assuming that demands in $E$ and $Q$ are the same in the four stages with light colors, and different shaded areas in Fig. 4.5(a)-4.5(d) illustrate different restorative zones from the three generators. Take Fig. 4.5(a) as an example. We know that in state 1, load buses $1, 2, 3, 4$ are in the same restorative zone supported by the generation MT. In the first stage, the MT can only provide 100 kW to the bus with the highest priority $\alpha_i$. It can be seen that the restored loads are increasing as the time evolves,

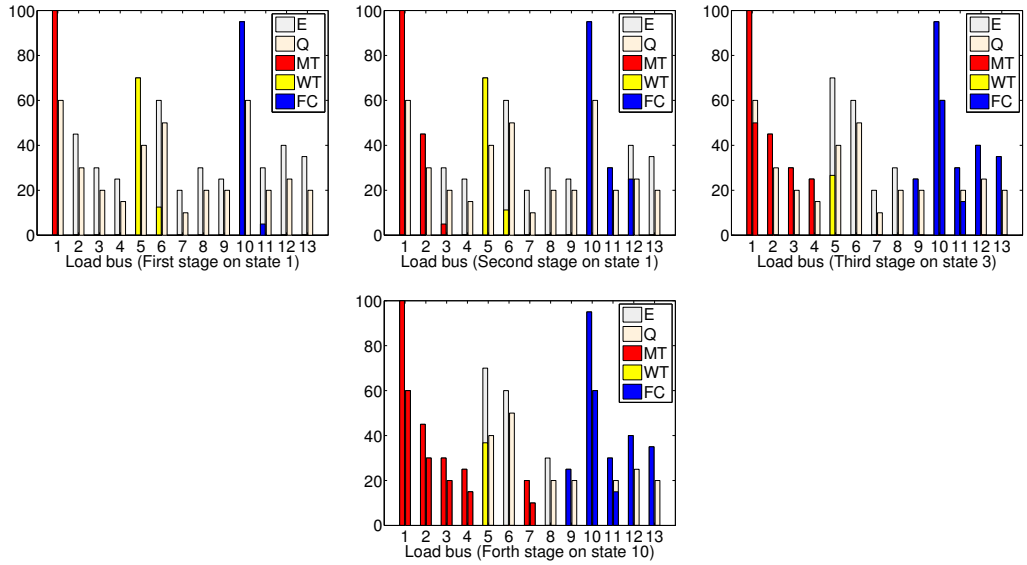


Figure 4.5: Restored loads (kW) scheduled on different load buses in four stages with shortest path states $1, 1, 3, 10$.

Table 4.3: Comparison of three scheduling methods

| Ps | Results of Different Methods | | | | | |
|---|---|---|---|---|---|---|
| | Method I | Method II | PH ($\rho = 100$) | PH ($\rho = 15000$) | PH (variable $\rho = c_s/(x_{max} - x_{min} + 1)$[65]) | Optimal Value |
| [0.1, 0.4, 0.3, 0.2] | 83272 | 83505 | 83304 | 83154 | 83154 | 83683 |
| [0.7, 0.1, 0.1, 0.1] | 48681 | 48797 | 48684 | 48684 | not converged | 48878 |
| [0.1, 0.2, 0.3, 0.4] | 98043 | 98016 | 97537 | 97537 | 97537 | 98325 |
| [0.1, 0.1, 0.1, 0.7] | 113300 | 112800 | 111450 | 111880 | 111880 | 113300 |
| [0.25, 0.25, 0.25, 0.25] | 80302 | 80269 | 79986 | 79986 | not converged | 80472 |

due to the fact that the synchronized generations from the MT and FC are growing.

### 4.4.2 Comparison of Two Scheduling Methods on Different $P_s$

The comparison between **Method I** and **Method II** is provided in Table 4.3. The numbers in the table are the results for the objective functions. The optimal solution is obtained by the brute-force method, which is not efficient especially when the state and stage numbers are large. It can be seen that both the proposed methods are sub-optimal. The reason for this is not the process of **Step 1**, which can provide us the optimal solution $(\mathbf{u}, \mathbf{v})$ for each time stage. The reason is due to the scenario bundle constraints resulting from the uncertainties of disconnection duration. **Method II** outperforms **Method I** when the

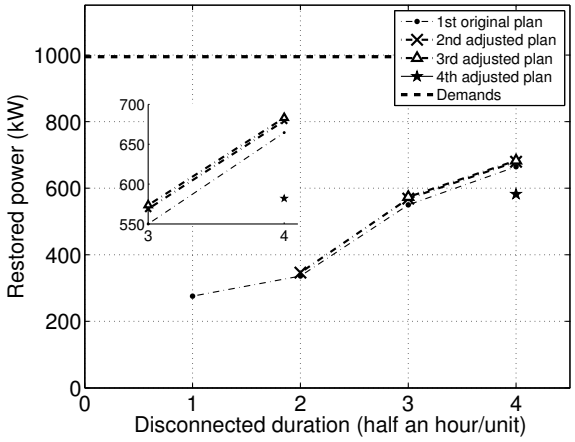


Figure 4.6: Adjustments on different forecasting horizons.

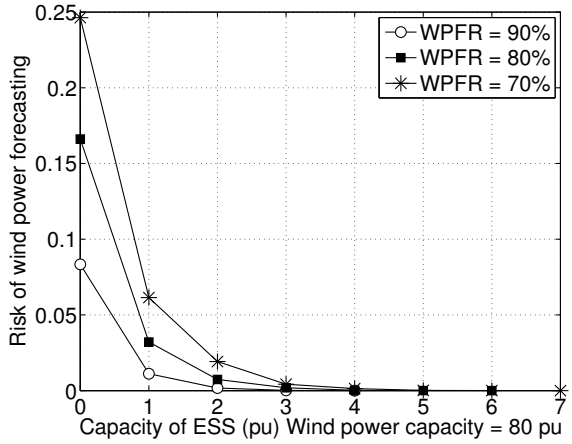


Figure 4.7: Impact of ESS on the risk of unreliability of WTs, with wind power capacity=80 pu.

frontal cases have greater probability of occurrence, especially in the first two cases. Since **Method II** is to solve the whole problem sequentially starting with scenario 1, and the following cases would follow the optimal solutions in the previous scenarios, the result will be better if the breakdown happens more frequently with shorter durations. In contrast, **Method I** is an averaged result of each independent case. As for the PH method, a different initial parameter $\rho$ leads to different results and even when we use the "variable-specific $\rho$" in [65], convergence is not guaranteed. The results of the proposed two methods are shown to be closer to the optima, while PH yields inferior solutions. Besides, it takes around 4

secs to do the simulation with PH while the proposed methods consume 1.5 and 1.6 secs, respectively, with the same parameters. The computer used is a ThinkPad Laptop with a i7 M560 duo-core processor at 2.67 GHz.

### 4.4.3 Adjustment of the Restoration Plan and the Effects of the ESS

The uncertainties of the wind power generation will pose negative impacts on the accuracy of the restoration scheme. With the linear standard variation assumption in Section 4.4.1, Fig. 4.6 examines the alternative restoration scheduling plans on different initial points. The original scheduling plan is adjusted with the time evolution. As the initial point moves forwardly, the estimated restored loads can be more accurate due to the fact that the uncertainties of the wind power estimation is smaller. Fig. 4.7 illustrates the impact of ESS on dealing with the errors of wind power forecasting. We assume that a fixed amount of energy is stored in the ESS immediately after the breakdown. The ESS will be functioning in the discharging state when the real wind power of the instant is smaller than $G_w$, until the stored energy is used up during the breakdown, and then be in the charging function the other way round. The risk of wind power forecasting is the simulated probability when the sum of the real wind power generation and the contribution of the ESS is less than the target wind power generation, $G_w$. It can be seen from Fig. 4.7 that the risk caused by unreliable wind power generation decreases with the growth of the ESS's capacity, and here pu values are provided for the capacity of ESS and the wind power capacity. Although the complete characteristic of a per-unit (pu) system requires that all four base values be defined, e.g., voltage, current, power, impedance, we consider the power scheduling and distribution here. The base power is set to be 1 pu=5 kW. A huge drop of risk takes place when the wind power capacity (80 pu) is supported by a small capacity (1 pu) of the ESS. This feature provides a guideline for determining the ESS size to deal with the inaccuracy of the forecasting.

## 4.5 Conclusions

This chapter has presented two sub-optimal yet efficient solutions for service restoration in a MG with unscheduled disconnection from the main grid, which can be computed by a two-step procedure efficiently based upon the stochastic information. Our study illustrates that both methods can obtain solutions very close to the optimal. From the simulation results, it can be seen that the ESS plays a critical role in decreasing the negative impacts from uncertainties of the forecasted renewable power generation.

# Chapter 5

# Pricing and Revenue Maximization for Battery Charging Services in PHEV Markets

In previous chapters, we have studied some scheduling optimization problems in the micro-grid. In this chapter, we focus on the charging services with pricing strategy in the plug-in hybrid electrical vehicle (PHEV) market from an economic perspective. The PHEV has shown great promise in the evolution of green energy, and becomes a critical part in the concept of the smart grid. We propose a piecewise linear quality of service model, and study the existence, uniqueness of the subscriber equilibrium, and the convergence of the subscriber dynamics.

## 5.1 Introduction and Motivation

Building a widespread infrastructure enabling battery charging at convenient locations such as road sides and parking lots stands as a promising solution to enable broad adoption of PHEVs [66, 67, 68]. The solution concept of charging stations offers a number of advantages

over that of individual household charging. First, the power needed for charging a PHEV is almost equal to the energy used in all appliances in a household, implying that large penetrations of PHEVs can create a non-negligible share of electricity demand which will drastically exacerbate the already high demand [69], [70]. Second, installing distributed charging stations are both convenient and necessary solutions for long-distance travelers who have no access to fixed charging facilities. Third, while charging in the dwelling unit is an option for individual householders, it is infeasible for people living in apartments and multi-family units, not to mention for some developing countries, where citizens even have no conditions to charge at home [68]. Therefore, we believe charging stations is a promising solution to promote the penetration of PHEVs in the near future.

We assume that charging service providers (CSPs) in the charging service market have the similar role and effect as the electric utilities and petroleum companies in some countries, more or less controlled by the government to be qualified to have the customer base, infrastructure, capital and ability to amortize the costs. There are two types of charging services that are currently envisioned to be implemented by the CSPs [67],[71]. One is a battery exchange service, denoted by $S_1$, which swaps a vehicle's depleted battery for a fully-charged battery. This service class has zero battery charging wait time for customers and allows the CSP to reap the benefits from lower-priced battery charging during valleys in the load profile and generates revenue from swapping services during daily business hours [69]. Practical examples include the Power Exchange Package system developed by Aurica Motors [67] . And it is assumed that the cost for the storage of battery and disposal of dead batteries from CSP will be covered by the government, not considered in this work. The other one is a battery charging service, denoted by $S_2$, which requires the customers to park their cars with close to depleted batteries at the charging station for a charging period. Depending on the selected charging voltage and facility setup, the charging time could range from 15 minutes (level 3 fast charging) to several hours (level 1 slow charging) [66]. For example,

in France, EDF and Toyota are currently installing level 2 charging stations for PHEVs on roads, streets and parking lots [72].

In this work, we investigate the pricing strategies of maximizing revenue for CSPs in PHEV charging service markets, possibly offering both battery swapping and charging services ($S_1$ and $S_2$). Meanwhile, we do not eliminate the possibility that some consumers would charge their PHEVs at dwelling units, which does not affect the results of this work. Our work is also closely related to several economic studies in diverse fields, such as [73, 74] focusing on the Paris Metro Pricing (PMP) and marginal user principle. Building upon the basic characteristics of Lithium-ion batteries, we incorporate the average waiting time in the system as the quality of service (QoS), and extend the commonly adopted linearly degrading QoS model in [75] to a general piecewise form.

## 5.2 Problem Formulation

Consider an electricity market with one CSP that offers two types of PHEV charging services, which differ in their prices and the corresponding QoS. A CSP serves each customer with a QoS, which is related to the average-waiting-time (QoS $\propto 1/$(average-waiting-time)) affected by both the waiting time in the queue and charging time in the chargers. We assume that the CSP is resource-constrained so that the corresponding QoS is generally a non-increasing function in terms of the number of subscribers. Over a discretized set of time indices, the customers in the market make decisions, by either opting out or opting for one of the services provided by this CSP, taking into account both the charged prices and QoS of the service classes. This dynamic process is commonly referred to as subscription dynamics.

We assume that the number of chargers in the station is $n$, which is chosen not to exceed the power limit in the whole system. Denote $\lambda_i$ as the fraction of customers that subscribes to service $S_i$ for $i = 1, 2$, and $q_i(\lambda_i)$ the corresponding QoS offered by the CSP. From the

discussion above we know that the user subscription profile satisfies $\lambda_1 + \lambda_2 \leq 1$ with $\lambda_i \in [0, 1]$. For the battery exchange service, since battery swapping can be normally accomplished in the order of several minutes [67], $q_1$ is modeled as a constant function independent of $\lambda_1$. The QoS of the battery charging service $q_2$ is more complicated. When the number of the customers (batteries to be charged) is less than the number of the available chargers, the QoS can be modeled as a constant function that reflects the average charging time[1]. Otherwise, when the system is overloaded, the charging process can be modeled as an $M/M/n$ queue. Strictly speaking, QoS is inversely proportional to and hence monotonically decreases with the fractions of customers $\lambda$. To obtain analytical insights and as in [73, 74, 75, 77], a linearly decreasing QoS function with respect to $\lambda$ is adopted to model the service capacity of the overloaded charging system. Other forms of decreasing QoS functions can be solved in a similar manner to the linear case. Therefore, $q_2(\lambda_2)$ is a piecewise and continuously semi-differentiable function[2] of the fraction of subscribers $\lambda_2$. An exemplary QoS function for $q_2$ is depicted in Fig. 5.1. The proof of the piecewise function of Qos model in Service 2 is as follow.

Proof: The QoS function defined in this chapter is inversely proportional to the average waiting time of PHEV charging versus the number of customers using the service. The average waiting time is composed of the average waiting time in a queue and the actual average charging time of the battery. We now explain why a two segment piecewise linear QoS function as shown in Fig. 5.1 can be used to model PHEV charging. In practice, the chargers can be connected in different ways in the charging stations, and without loss of generality we consider the common connection circuit, parallel charging style in this emerging charging service market. Based upon the charging features of Lithium-ion batteries [78], the relation between the QoS, (i.e., QoS $\propto 1/$(average-waiting-time)) and the fraction of customers $\lambda$ is

[1]It can be easily shown for a parallel charging circuits, that the battery charging time is solely determined by the charging voltage and is independent of the number of batteries currently charged in the system [76].

[2]A continuously semi-differentiable function contains possibly a finite number of non-differentiable points and is left as well as right differentiable at all the non-differentiable points.

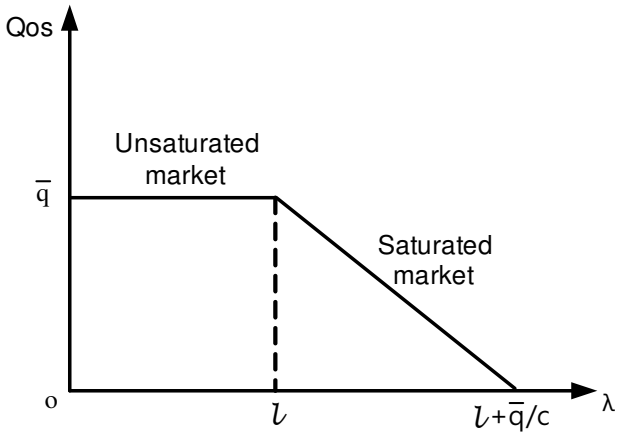


Figure 5.1: QoS function model for parallel battery charging service $S_2$ (with $l$ being the transition point indicating the number of chargers in the market, $c$ the parameter indicating the QoS degrading speed, $\bar{q}$ the maximum QoS value of $S_2$).

modeled as in Fig. 5.2.

**1) Constant QoS part in Fig. 5.1.** This case represents the number of customers (batteries to be charged) is less than the number of available chargers, and there is no waiting time in the queue. To prove this, we are going to show that in parallel charging circuit, the average charging time for a specific user is constant and independent of the number of the batteries paralleled in the system.

When a battery is charged in a charger, it can be treated as a capacitor [78], and the charging procedure can be regarded as the step response of the circuit due to a sudden application of a dc voltage (or current) source. Figure 5.2 represents a "Step Response of a RC Circuit", which is the circuit model of our case. $V_s$ is a constant, dc voltage source. We first select the capacitor voltage as the circuit response to be determined, then assume an initial voltage $V_0$ on the capacitor. Since the voltage of a capacitor cannot change instantaneously, we have $v(0^-) = v(0^+) = V_0$, where $v(0^-)$ is the voltage across the capacitor before switching and $v(0^+)$ is its voltage immediately after switching. Applying Kirchhoff's First Law (KCL), we have

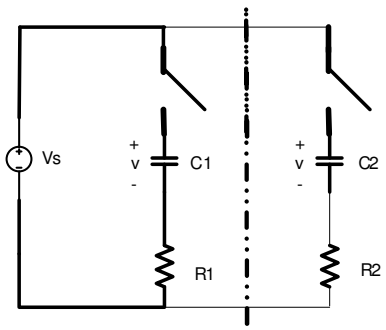


Figure 5.2: RC circuit with voltage step input

.

$$C_1 \frac{dv}{dt} + \frac{v - V_s u(t)}{R_1} = 0, \tag{5.1}$$

or

$$\frac{dv}{dt} + \frac{v}{R_1 C_1} = \frac{V_s}{R_1 C_1}, \text{ for } t > 0, \tag{5.2}$$

where $v$ is the voltage across the capacitor. Then we have,

$$\frac{dv}{v - V_s} = -\frac{dt}{R_1 C_1}. \tag{5.3}$$

Integrating both sides and introducing the initial conditions, there is

$$\ln(v - V_s) \mid_{V_0}^{v(t)} = -\frac{t}{R_1 C_1} \mid_0^t \tag{5.4}$$

or

$$\ln \frac{v - V_s}{V_0 - V_s} = -\frac{t}{R_1 C_1}, \tag{5.5}$$

Then we have,

$$\frac{v - V_s}{V_0 - V_s} = e^{-t/\tau_1}, \text{ with } \tau_1 = R_1 C_1. \tag{5.6}$$

and

$$v(t) = V_s + (V_0 - V_s) e^{-t/\tau_1}, \text{ for } t > 0. \tag{5.7}$$

Correspondingly, the current response is given by

$$i(t) = \frac{(V_s - V_0) \exp(-\dfrac{t}{\tau_1})}{R_1}, \qquad t > 0. \tag{5.8}$$

When another capacitor is paralleled to the charging circuits, the voltage on each branch is the same, and then we have

$$V_s = i_1(t) R_1 + \frac{1}{C_1} \int_0^t i_1(\tau) d\tau = i_2(t) R_2 + \frac{1}{C_2} \int_0^t i_2(\tau) d\tau. \tag{5.9}$$

Taking the derivative with respect to $t$, we obtain

$$0 = C_1 R_1 \frac{di_1(t)}{dt} + i_1(t) = C_2 R_2 \frac{di_2(t)}{dt} + i_2(t), \tag{5.10}$$

with the initial current $i_1(0) = \frac{V_s - V_{01}}{R_1}$, $i_2(0) = \frac{V_s - V_{02}}{R_2}$, and $V_{01}$, $V_{02}$ are initial voltages on the different capacitors, respectively. The solutions to the differential equations (10) are given by

$$i_1(t) = (V_s - V_{01}) \exp(-\frac{t}{\tau_1})/R_1, \tag{5.11}$$

$$i_2(t) = (V_s - V_{02}) \exp(-\frac{t}{\tau_2})/R_2. \tag{5.12}$$

Note that (5.11) is equal to (5.8). Based upon the characteristic of the Li-ion battery, the charging time is only dependent on the charging current to a specific battery, indicating that the average service time in this case is constant and irrelevant to the number of users. This explains the constant part of QoS in Fig. 5.1.

**2) Linearly decreasing QoS part in Fig. 5.1.** This case represents the number of customers (batteries to be charged) is larger than the number of available chargers. To prove this, we first embark on showing that the charging process in this case can be modeled as a $M/M/n$ queue, and then show why the QoS function is approximated by a linearly decreasing function with respect to $\lambda$.

Classical queuing theory models the number of customers arriving at a queue by a Poisson process with arrival rate $\gamma$. In our PHEV charging system, the customer arrival interval $t$ meets the properties of the exponential distribution, leading to a Poisson arrival process. In practice, the batteries to be charged in the system have different battery properties such as capacity, amount needed to be charged, maximum power, etc, so the service time $\tau$ of the PHEVs are independently and identically distributed (iid) as exponential distribution. Furthermore, the charging system has a threshold number of PHEVs that can be charged

simultaneously (the maximum number of chargers), denoted by $n$. Therefore, the charging process in this case can be regarded as an $M/M/n$ queue. In the mathematical theory of queues, Little's law states that the long-term average number of customers $\lambda$ in a stable system is equal to the long-term average effective arrival rate $\gamma$, multipled by the average waiting time $Q$ a customer spends in the system, that is: $\lambda = \gamma Q$. Note that $Q$ is the average waiting time inversely proportional to the QoS in our work, and $\lambda$ can be seen as the fractions of customers that subscribe to the charging service. Strictly speaking, QoS is inversely proportional to and hence monotonically decreases with the fractions of customers $\lambda$. To obtain analytical insights, a linearly decreasing QoS function with respect to $\lambda$ is adopted to model the service capacity of the overloaded charging system. Other forms of decreasing QoS functions can be solved in a similar manner to the linear case.

■

The users can subscribe potentially to one of the services for battery charing. As in [73, 75], we assume the subscribers follow a continuum model[3] and are of diversity, meaning that they can value the same level of QoS differently. Specifically, each user is characterized by a QoS valuation parameter $\theta$, which has positive and continuous probability density function $f(.)$ taking value in $[0, \beta]$ with $\beta > 0$. For instance, a uniformly distributed $\theta$ means that the users are fully diversified in the sense that there exist users that are totally indifferent to service QoS ($\theta \to 0^+$) and the ones that value the QoS considerably ($\theta \to \beta^-$). Moreover, the fractions of users in each category are identical on an average sense. Thus, the utility achieved by user $k$ subscribing to service $S_i$ can be expressed as

$$u_{k,i} = \theta_k q_i(\lambda_i) - p_i, \tag{5.13}$$

where $\theta_k$ is the QoS valuation parameter of user $k$, and $p_i$ is the price charged by the CSP

[3]The continuum model has been widely used in the literature of economics to approximate large user populations [74].

for service $S_i$. The utility function represents the preference of a user over some service, which equals the difference between the service QoS (as weighted by a subjective valuation parameter) and the charged price.

Given the superiority of $S_1$, it is natural to assume that $S_1$ provides better QoS than $S_2$ and charges a higher price. Mathematically, we have $q_1 > q_2(\lambda_2)$ for all $\lambda_2 \in [0, 1]$ and $p_1 > p_2$. The customers are assumed to be rational in the sense that before they make subscription decisions, they would compare and choose the service that delivers a higher utility. Mathematically, user $k$ prefers $S_i$ to $S_j$ only if $u_{k,i} > u_{k,j}$ and $u_{k,i} > 0$, where $i, j \in \{1, 2\}$ [74]. When the utilities of both services are negative, the customers will subscribe to neither of the services and prefer charing at their own dwelling units. In this work, we assume that users who subscribe to neither of the two services gain zero utility.

## 5.3 Subscription Dynamics and Revenue Maximization: Single Service Case

Note that in the single service case, the service index (subscript $i$) is omitted for notation simplicity.

### 5.3.1 Semi-Differentiable QoS Function: The General Case

Let us consider a monopoly charging service market with a CSP operating a single service $S$. The QoS function of $S$, denoted by $q(\lambda)$, is considered to be a semi-differentiable function and non-increasing in $\lambda$. The time is assumed to be discretized as $t = 0, 1, 2, ...$ and $\lambda^{(t)}$ the fraction of subscribers to $S$ with $\lambda^{(0)}$ denoting the initial fraction. At each time instance $t$, user $k$ makes a subscription decision individually to maximize its utility in the current time instant. In particular, by evaluating the utility function (5.13), user $k$ will subscribe to service $S$ if and only if the utility $u_k^{(t)}$ is non-negative. Due to causality, we assume that

each user expects QoS in the current time instant $\tilde{q}\left(\lambda^{(t)}\right)$ to be equal to that in the previous instance, i.e., $\tilde{q}\left(\lambda^{(t)}\right) = q\left(\lambda^{(t-1)}\right)$. Thus, the fraction of subscribers to $S$ at time instant $t$ is given by

$$\lambda^{(t)} = \mathbb{P}\left[u_k^{(t)} \geq 0\right] = \mathbb{P}\left[\theta_k \geq \frac{p}{q\left(\lambda^{(t-1)}\right)}\right] = 1 - F_\theta\left(\frac{p}{q\left(\lambda^{(t-1)}\right)}\right) \triangleq h\left(\lambda^{(t-1)}\right), \tag{5.14}$$

where $\mathbb{P}[\cdot]$ is the probability operator, $p$ the price of $S$, and $F_\theta(.)$ is the cumulative distribution function (CDF) of the QoS valuation parameter $\theta$. Then, $\lambda^{(t)}$ evolves following a sequence $\left\{\lambda^{(t)}\right\}_{t=0}^{\infty}$ in $[0, 1]$. What we are interested in is whether the subscriber dynamic (5.14) is a convergent process. To this end, we define the equilibrium point of the user subscription dynamics.

**Definition 1.** $\lambda^*$ is an equilibrium point of the user subscription dynamics in the single service market of a CSP if it satisfies the fixed-point equation $h(\lambda^*) = \lambda^*$.

**Theorem 1.** For any non-negative price $p$, there exists a unique equilibrium point $\lambda^*$ to the subscriber dynamics (5.14) in a monopoly market with a single service $S$. The proof is as follows.

Proof: Theorem 1 establishes the existence and uniqueness of the equilibrium point of the fixed point equation given in Definition 1 and generalizes the result in [73] to the case of semi-differentiable QoS functions.

Denote $g(\lambda) = h(\lambda) - \lambda$. To prove the uniqueness of the equilibrium point, equivalently, we show that the equation $g(\lambda) = 0$ has a unique feasible solution. Given that $q(\cdot)$ is non-increasing, it is not difficult to verify that $g(\cdot)$ is strictly decreasing in $[0, 1]$. Next, we have $g(0) = h\left(\frac{p}{q(0)}\right) > 0$ and $g(1) = -F\left(\frac{p}{q(1)}\right) < 0$. Given that $h(\cdot)$ is continuous on $[0, 1]$, it follows that $g(\cdot)$ has a unique root on $[0, 1]$ by the intermediate value theorem, which establishes the uniqueness of the equilibrium point. ■

To establish the convergence property of the subscriber dynamics, we introduce Definition

2.

**Definition 2.** Denote $\mathbf{dom}\, f$ as the domain of the function $f$. A subderivative of the function $f : R \to R$ at a point $z \in \mathbf{dom}\, f$ is a real number $\phi(z)$ such that $f(x) - f(z) \geq \phi(z)(x - z)$. The set of subderivatives of $f$ at the point $z$ is called the subdifferential of $f$ at $z$, denoted by $\partial f(z)$.

**Theorem 2.** For any price $p$, the subscriber dynamics converge to the unique equilibrium point from an arbitrary start point, if the following condition is satisfied

$$\max_{\substack{\lambda\in[0,1]\\ \phi(\lambda)\in\partial q(\lambda)}} -f\left(\frac{p}{q(\lambda)}\right)\frac{p}{q(\lambda)}\frac{\phi(\lambda)}{q(\lambda)} < 1, \tag{5.15}$$

where $\phi(\lambda)$ is a subderivative of $q(\cdot)$ at $\lambda$, $\partial q(\lambda)$ the subdifferential of $q(\cdot)$ at $\lambda$, which takes value in the set $[\min(q'(\lambda^-), q'(\lambda^+)), \max(q'(\lambda^-), q'(\lambda^+))]$, where $q'(\lambda^-)$ and $q'(\lambda^+)$ are left and right derivatives of $q(.)$, respectively. The proof is as follows.

Proof: When the QoS function is continuously differentiable, one can resort to contraction mapping theory and the mean value theorem to derive sufficient conditions that guarantee convergence, as in [75]. Nevertheless, the techniques are not readily applicable when the QoS function contains a finite number of non-differentiable points. We overcome this difficulty by resorting to the concept of superdifferentiability.

Let $\lambda_a$ and $\lambda_b$ be two different real numbers arbitrarily chosen from the interval $[0, 1]$ and suppose without loss of generality that $\lambda_a > \lambda_b$. We illustrate the important proving steps by focusing on the case $\frac{p}{q(\lambda_a)} < \beta$ and $\frac{p}{q(\lambda_b)} < \beta$ with $p > 0$ (the other cases can be trivially proved). We shall show that the function $h(\cdot)$ is a contraction mapping on $[0, 1]$ with respect to the absolute value norm if (5.15) in the main text is satisfied.

Given that $h(\cdot)$ is semi-differentiable on $(\lambda_a, \lambda_b)$, by the mean value theorem, there exist

$\lambda_c \in (\lambda_a, \lambda_b)$ and a superderivative $\tilde{\phi}(\lambda_c) \in \partial q(\lambda_c)$ such that

$$\begin{aligned} & |h(\lambda_a) - h(\lambda_b)| \\ = \; & |h'(\lambda_c)||\lambda_a - \lambda_b| = \left| f\left(\frac{p}{q(\lambda_c)}\right) \frac{p}{q(\lambda_c)} \frac{\tilde{\phi}(\lambda_c)}{q(\lambda_c)} \right| |\lambda_a - \lambda_b| \\ \leq \; & \kappa_m |\lambda_a - \lambda_b|. \end{aligned} \tag{5.16}$$

Then, it is clear that if (5.15) is satisfied, i.e., $\kappa_m < 1$, the mapping $h(\cdot)$ is a contraction mapping. The other cases can be proved similarly, which completes the proof. ■

### 5.3.2 Piecewise Linear QoS Function: PHEV Charging Service Case

Based on the general QoS function results above, we study in this subsection a piecewise linear QoS function, depicted in Fig. 5.1, which describes the QoS of a normal battery charging service in PHEV markets.

**Definition 3.** The market is said to stabilize at an *unsaturated* state if the fraction of subscribers is no more than the transition point ($\lambda \leq l$). It is said to be at a *saturated* state if the fraction of subscribers exceeds the transition point ($\lambda > l$). The transition point $l$ is the normalized number of chargers for $S_2$ in the system.

Mathematically, the piecewise linear QoS function can be expressed as

$$q(\lambda) = \begin{cases} \overline{q}, & \lambda \leq l, \\ \overline{q} + c(l - \lambda), & \text{Otherwise} \end{cases} \tag{5.17}$$

where $\overline{q}$ is the QoS of the unsaturated market, $l$ the transition point where the two sections of the QoS function meet, and the parameter $c \in (0, \infty)$ indicates the QoS degrading speed. The equilibrium points that correspond to both cases can be obtained by solving the fixed-

point equation $\lambda^* = h(\lambda^*)$, which yields

$$\lambda^* = \begin{cases} \left(1 - \dfrac{p}{\beta \overline{q}}\right)^+, & \lambda^* \in [0, l], \\ \left(\dfrac{\overline{q} + cl + c - \sqrt{(\overline{q} + cl - c)^2 + 4cp/\beta}}{2c}\right)^+, & \lambda^* \in (l, 1]. \end{cases} \tag{5.18}$$

In what follows, we shall strengthen Theorem 2 by deriving a sufficient and necessary condition for the convergence of the user dynamics under the assumption that the QoS valuation parameter $\theta$ is uniformly distributed, i.e., $f(\theta) = 1/\beta$, where $\beta > 0$.

**Theorem 3.** Suppose that in a PHEV market, the initial fraction of subscribers $\lambda^{(0)} \in [0, l]$ and the QoS valuation parameter $\theta$ is uniformly distributed. Then, for a given service price $p$ and QoS function given by (5.17), the subscriber dynamics converge to a unique equilibrium point, if and only if either condition is satisfied $l \geq 1 - \frac{p}{\beta \overline{q}}$ or $1 - \frac{\overline{q}}{c} < l < 1 - \frac{p}{\beta \overline{q}}$. The proof is as follow.

Proof: We introduce the following lemma, which is the basic condition of Theorem 3.

**Lemma 1.** 1) $h(x)$ is non-increasing, 2) If $\lambda^{(0)} \in [0, l]$ and $\lambda^{(1)} \in (l, 1)$, then $\lambda^* \in \left(l, \lambda^{(1)}\right]$.

The non-increasing property of $h(x)$ can be proved easily by exploring the monotonicity properties of the QoS function $q(.)$ and the CDF of the QoS valuation parameter $\theta$, $F(.)$. Next, given $\lambda^{(1)} \in (l, 1]$, let us first hypothetically assume that the equilibrium point $\lambda^* \in (0, l]$. Then, based on (5.18), we have

$$\lambda^{(1)} = h\left(\lambda^{(0)}\right) = 1 - \frac{p}{\beta \overline{q}} \quad > \quad l, \tag{5.19}$$

$$\lambda^* = \frac{\overline{q} + cl + c - \sqrt{(\overline{q} + cl - c)^2 + 4cp/\beta}}{2c} \quad \leq \quad l. \tag{5.20}$$

It follows from (5.20) that $l \geq 1 - p/(\beta \overline{q})$, which contradicts (5.19). Therefore, we know that $\lambda^* \notin (0, l]$, i.e., $\lambda^* > l$. Next, given that $\lambda^{(0)} \in [0, l]$, we have $\lambda^* = h(\lambda^*) \leq h\left(\lambda^{(0)}\right) = \lambda^{(1)}$,

where the inequality follows from the non-increasing property of $h(x)$. Thus, we have proved that if $\lambda^{(0)} \in [0, l]$ and $\lambda^{(1)} \in (l, 1)$, then $\lambda^* \in \left(l, \lambda^{(1)}\right]$.

Given the initial subscriber fraction $\lambda^{(0)}$, the proof is accomplished by considering three cases of the relationship between the user fractions in the following two consecutive time instances, i.e., $\lambda^{(1)}$ and $\lambda^{(2)}$.

*Case 1* $\left(\text{if } \lambda^{(1)} \in (0, l]\right)$: Given that $\lambda^{(0)} \in [0, l]$, we have $\lambda^{(1)} = h(\lambda^{(0)}) = \lambda^* \in (0, l]$.

*Case 2* $\left(\text{if } \lambda^{(1)}, \lambda^{(2)} \in (l, 1]\right)$: Given that $\lambda^{(0)} \in [0, l]$ and Lemma 1, we know $\lambda^{(2)} = h(\lambda^{(1)}) \leq h(\lambda^*) = \lambda^*$. Since $\lambda^{(2)} \in (l, 1]$, we have $\lambda^{(2)} \in (l, \lambda^*]$. Next, we have

$$\lambda^* = h(\lambda^*) \leq h(\lambda^{(2)}) = \lambda^{(3)} \leq h(\lambda^{(0)}) = \lambda^{(1)}. \tag{5.21}$$

We then split the iteratively generated sequence $\left\{\lambda^{(t)}\right\}$ into two subsequences

$$\text{Subsequence A} : \left\{\lambda^{(2t)} \middle| t \in \mathbb{N}\right\} = \left\{\lambda^{(0)}, \lambda^{(2)}, ..., \lambda^{(2t)}, ...\right\}, \text{ and}$$
$$\text{Subsequence B} : \left\{\lambda^{(2t+1)} \middle| t \in \mathbb{N}\right\} = \left\{\lambda^{(1)}, \lambda^{(3)}, ..., \lambda^{(2t+1)}, ...\right\}.$$

Without loss of generality, we prove the global convergence of subsequence B by induction. Given that $\lambda^* \leq \lambda^{(3)} \leq \lambda^{(1)}$, suppose that for $t > 1$, $\lambda^{(2t+1)} \leq \lambda^{(2t-1)}$. Then, we have

$$\lambda^{(2t+3)} = h\left(h\left(\lambda^{(2t+1)}\right)\right) \overset{(a)}{\leq} h\left(h\left(\lambda^{(2t-1)}\right)\right) = \lambda^{(2t+1)}, \tag{5.22}$$

where $(a)$ follows from the non-increasing property of $h(\cdot)$, as proved in Lemma 1. Thus, we have shown that subsequence B is a monotonically decreasing sequence lower bounded by $\lambda^*$, which implies subsequence B is a converging sequence. The convergence property of subsequence A can be established similarly. To this end, $\lambda^* \in (l, \lambda^{(1)})$.

*Case 3* $\left(\text{if } \lambda^{(1)} \in (l, 1], \lambda^{(2)} \in (0, l]\right)$: Similar to Case 2, we know that $\lambda^{(1)} = h(\lambda^{(0)})$. Given that $\lambda^{(2)} \in (0, l]$, we have $\lambda^{(3)} = h(\lambda^{(2)}) = h(\overline{q}) = \lambda^{(1)}$. Thus, in this case, the

subscriber dynamics will oscillate between the unsaturated state and the saturated state, or in other words, the market is unstable.

Therefore, the conditions under which Case 3 does not hold are the necessary and sufficient condition that guarantees convergence, given by Theorem 3. The first part of the condition can be easily derived based on $\lambda^{(1)} < l$ and the second part follows by solving $\lambda^{(1)} > l$ and $\lambda^{(2)} > l$. This completes the proof.

The above three cases portrait the complete picture of subscriber dynamics in all situations. Both Case 1 and Case 2 are convergent cases that differ in the number of iterations. Intuitively, we observe from the conditions that to ensure the convergence of subscriber dynamics, the service price $p$ should be set no less than a given threshold to prevent the market from oscillating between the unsaturated state and the saturated state. ■

### 5.3.3 Revenue Maximization

The next objective is to investigate the decision of an optimal service price, denoted by $p^{\dagger}$, which maximizes the revenue of the CSP. Recall that the market can stabilize at two different states as in (5.18), we shall study both cases one by one and obtain the optimal prices and the corresponding maximum revenues, followed by the discussion of some interesting insights for the CSP. The revenue of a CSP at price $p$ can be expressed as in [75], with no consideration of cost:

$$R(p) = p\lambda^{*}(p), \tag{5.23}$$

where $\lambda^{*}(p)$ is the equilibrium point of the user subscription at price $p$. Besides, we use $R_{I}^{\max}$ and $R_{II}^{\max}$ to denote the maximum revenue corresponding to an unsaturated market and a saturated market, respectively. Without loss of generality, we set the distribution parameter $\beta = 1$ in the following analysis, which means $F_{\theta}(\theta) = \theta$ for $\theta \in [0, 1]$.

**Unsaturated Market** ($\lambda^* \in [0, l]$)

A constrained revenue maximization problem based on (5.23) becomes: $\underset{p}{\text{maximize}}\ p(1-p/\overline{q})$, subject to $1 - p/\overline{q} \leq l$. Accordingly, the maximum revenue in an unsaturated market, $R_I^{\max}$, can be expressed as

$$R_I^{\max} = \begin{cases} l(1-l)\overline{q} & \text{if } l \leq 1/2, \\ \overline{q}/4 & \text{Otherwise,} \end{cases} \tag{5.24}$$

with $p^\dagger = \max(1-l, 1/2)\overline{q}$. The corresponding curve is plotted in Fig. 5.3 (the dotted square curve) as a function of the transition point $l$.

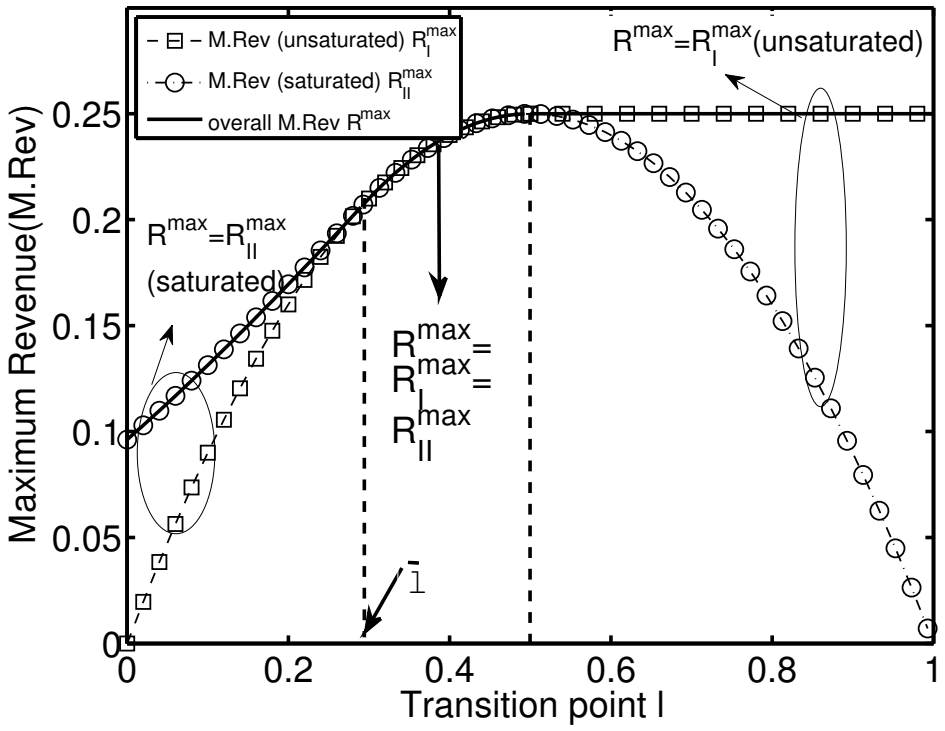


Figure 5.3: The maximum revenue for the CSP in a single service market with $c = 2$ and $\overline{q} = 1$.

**Saturated Market** ($\lambda^* \in (l, 1]$)

In a saturated market, the revenue optimization problem based on (5.23) and (5.18) directing solving for $p^\dagger$ is non-convex, and a closed-form solution is mathematically intractable. To this end, we resort to the marginal user principle[4] introduced in [73, 74, 75]. Suppose that a marginal user exists in this work, and assuming user $j$ is the marginal user. Then, we have $u_j = \theta_j q - p = 0$, which means $\theta_j = p/q$. Besides, we have $\lambda^* = 1 - F_\theta(p/q) = 1 - \theta_j$ and thus $\max_p p\lambda^*(p) = \max_\theta \theta q(\theta)(1-\theta)$. The optimal solution for $\theta^\dagger$ can be obtained in closed form by applying the Karush-Kuhn-Tucker (KKT) conditions, and therefore the optimal price is given by $p^\dagger = \min\big(\tilde{\theta}^\dagger(\overline{q} + c(\tilde{\theta}^\dagger + l - 1)), (1-l)\overline{q}\big)$. Accordingly, the maximum revenue, $R_{II}^{\max}$, can be calculated as follows, and the corresponding curve has been plotted in Fig. 5.3.

$$R_{II}^{\max} = \begin{cases} \tilde{\theta}^\dagger(\overline{q} + c(\tilde{\theta}^\dagger + l - 1))(1 - \tilde{\theta}^\dagger), & \text{if } l \le \bar{l}, \\ l(1-l)\overline{q}, & \text{Otherwise,} \end{cases} \tag{5.25}$$

where $\bar{l} = \frac{c + 2\overline{q} - \sqrt{c^2 + 4\overline{q}^2}}{2c}$, and $\tilde{\theta}^\dagger = \frac{2c - (\overline{q} + cl) + \sqrt{(\overline{q} + cl)^2 + c^2 - c(\overline{q} + cl)}}{3c}$.

**Remark 2** – Observe from Fig. 5.3 that the maximum revenue in an unsaturated market increases quadratically as the transition point $l$ increases, which levels off at the value of $\overline{q}/4$ when the transition point grows larger than $1/2$. This implies that there exists an upper limit on the amount investment (i.e., $l = 1/2$). In a saturated market, the trend of the maximum revenue $R_{II}^{\max}$ should be noted from (5.25) that as long as the amount of investment $l$ is larger than $\bar{l}$, the revenue-maximizing fraction of subscribers $\lambda^\dagger$ always equals the transition point $l$, which grows linearly as $l$ increases. Hence, the maximum revenue, $R^{\max}$ (the solid curve in Fig. 5.3), is given by the point-wise maximum of $R_I^{max}$ and $R_{II}^{\max}$,

[4]In the single service market of a CSP, marginal users are indifferent between participating and not participating in the service given the price $p$ and the current $q$. In our model, a marginal user receives zero utility.

which is summarized as

$$R^{\max} = \begin{cases} R_{II}^{\max} & l \in [0, \bar{l}), \\ R_{I}^{\max} = R_{II}^{\max} & l \in [\bar{l}, 1/2), \\ R_{I}^{\max} & l \in [1/2, 1]. \end{cases} \tag{5.26}$$

We observe from Fig. 5.3 that the maximum revenue $R^{max}$ can be divided into three parts: $l \in [0, \bar{l}], [\bar{l}, 1/2], [1/2, 1]$. The following conclusions can be drawn from the perspective of revenue maximization:

- For a small value of $l \in [0, \bar{l})$, the CSP should lower the service price to attract more subscribers.
- For an intermediate value of $l \in [\bar{l}, 1/2)$, the revenue-maximizing fraction of subscribers $\lambda^{\dagger}$ always equals the transition point $l$, which grows linearly as $l$ increases.
- To reach the maximum revenue $\overline{q}/4$, it suffices for the CSP to 1) ensure that the QoS function can accommodate half of the population without degrading the provided service quality and 2) select an optimal price so that exactly half of the population opt for the service.

## 5.4 Subscription Dynamics and Revenue Maximization: Duo-Service Case

In this section, we extend the above analysis to a charging service market with two different classes of services, referred to as a duo-service market that encompasses a battery swapping service $S_1$ and a battery charing service $S_2$. As in the single-service market case, we also assume that the users update their subscription decisions at discrete time indices $t = 1, 2, ...$, expecting the current QoS provided by the CSP is equal to the previous period. Moreover,

the users are rational and will always subscribe to the service class that provides a higher and positive utility value. Besides, other than the subscription fee ($p_1$ or $p_2$) and as in [75], we assume there is no cost for the decisions. In the presence of two different service classes, the population can be divided into three groups. One is the subscribers who choose $S_1$ in time index $t$ if and only if

$$\theta_k q_1 - p_1 \geq \theta_k q_2 \left(\lambda_2^{(t-1)}\right) - p_2 \text{ and } \theta_k q_1 - p_1 \geq 0, \tag{5.27}$$

another is the subscribers who choose $S_2$ if and only if

$$\theta_k q_2 \left(\lambda_2^{(t-1)}\right) - p_2 > \theta_k q_1 - p_1 \text{ and } \theta_k q_2 \left(\lambda_2^{(t-1)}\right) - p_2 \geq 0, \tag{5.28}$$

The rest of the population choose neither of the services and may opt for, e.g., charging at their own dwelling units. As in the single-service market, we study the existence and uniqueness of the equilibrium point.

**Theorem 4.** For any non-negative price pair $(p_1, p_2)$ and QoS pair $(q_1, q_2(\lambda_2))$ satisfying $p_1 > p_2$ and $q_1 > q_2(\lambda_2)$ for all $\lambda_2 \in [0, 1]$, there exists an equilibrium point $(\lambda_1^*, \lambda_2^*)$ of subscriber dynamics in the duo-service market which is also unique and is given by

$$(\lambda_1^*, \lambda_2^*) = \begin{cases} \left(1 - F_\theta(\frac{p_1}{q_1}), 0\right) & \text{if } \frac{p_1}{q_1} \leq \frac{p_2}{q_2(\lambda_2)}, \\ \left(1 - F_\theta\left(\frac{p_1 - p_2}{q_1 - q_2(\lambda_2^*)}\right), F_\theta\left(\frac{p_1 - p_2}{q_1 - q_2(\lambda_2^*)}\right) - F_\theta\left(\frac{p_2}{q_2(\lambda_2^*)}\right)\right) & \text{if } \frac{p_1}{q_1} > \frac{p_2}{q_2(\lambda_2)}, \end{cases} \tag{5.29}$$

The proof is as follows.

Proof: To prove the existence and uniqueness of the equilibrium point in a duo-service market, we shall first show that the equilibrium point can be derived as in (5.29), followed by a proof on its existence and uniqueness. We start by rewriting the subscriber preference (5.27) and (5.28). After some algebra, the condition that the subscriber opts for $S_1$ can be

equivalently expressed as

$$\theta_k \geq \max\left(\frac{p_1 - p_2}{q_1 - q_2(\lambda_2)}, \frac{p_1}{q_1}\right) \tag{5.30}$$

and the condition for opting for $S_2$

$$\frac{p_2}{q_2(\lambda_2)} < \theta_k < \frac{p_1 - p_2}{q_1 - q_2(\lambda_2)}. \tag{5.31}$$

Next, we derive the subscriber equilibrium in two different cases.

*Case 1* $\left(\text{if } \frac{p_1}{q_1} \leq \frac{p_2}{q_2(\lambda_2)}\right)$: Given that $p_1 > p_2 > 0$ and $q_1 > q_2(\lambda_2)$, it can be shown easily that $\frac{p_1-p_2}{q_1-q_2(\lambda_2)} \leq \frac{p_1}{q_1} \leq \frac{p_2}{q_2(\lambda_2)}$. Thus, based on (5.30) and (5.31), the fractions of subscriber to both services can be calculated as, respectively,

$$\lambda_1^{(t)} = 1 - F\left(\frac{p_1}{q_1}\right) \text{ and } \lambda_2^{(t)} = 0. \tag{5.32}$$

*Case 2* $\left(\text{if } \frac{p_1}{q_1} > \frac{p_2}{q_2(\lambda_2)}\right)$: Similar to *Case 1*, the following inequality can be derived $\frac{p_1-p_2}{q_1-q_2(\lambda_2^{t-1})} > \frac{p_1}{q_1} > \frac{p_2}{q_2(\lambda_2^{t-1})}$, based on which, together with (5.30) and (5.31), the fractions of subscriber to both services are, respectively,

$$\lambda_1^{(t)} = 1 - F\left(\frac{p_1 - p_2}{q_1 - q_2(\lambda_2^{t-1})}\right) \text{ and } \lambda_2^{(t)} = F\left(\frac{p_1 - p_2}{q_1 - q_2(\lambda_2^{t-1})}\right) - F\left(\frac{p_2}{q_2(\lambda_2^{t-1})}\right). \tag{5.33}$$

Therefore, the subscriber equilibrium is given by

$$(\lambda_1^*, \lambda_2^*) = \begin{cases} \left(1 - F(\frac{p_1}{q_1}), 0\right) & \text{if } \frac{p_1}{q_1} \leq \frac{p_2}{q_2(\lambda_2)}, \\ \left(1 - F\left(\frac{p_1-p_2}{q_1-q_2(\lambda_2^*)}\right), F\left(\frac{p_1-p_2}{q_1-q_2(\lambda_2^*)}\right) - F\left(\frac{p_2}{q_2(\lambda_2^*)}\right)\right) & \text{if } \frac{p_1}{q_1} > \frac{p_2}{q_2(\lambda_2)}. \end{cases} \tag{5.34}$$

Next, to show that the above equilibrium point (5.34) is unique, we note that the equilibrium point in *Case 1* follows naturally as $(1 - F(p_1/q_1), 0)$ is the unique solution. In terms of *Case 2*, the same line of proof in Theorem 1 can be used to show that the following equation has

a unique root ($\lambda_2^*$ is unique)

$$\lambda_2^* = F\left(\frac{p_1 - p_2}{q_1 - q_2(\lambda_2^*)}\right) - F\left(\frac{p_2}{q_2(\lambda_2^*)}\right). \tag{5.35}$$

Hence, $\lambda_1^*$ is also unique as

$$\lambda_1^* = 1 - F\left(\frac{p_1 - p_2}{q_1 - q_2(\lambda_2^*)}\right), \tag{5.36}$$

which completes the proof. ■

### 5.4.1 Revenue Maximization

To simplify parameter representation and without loss of generality, we assume $\beta = 1$ and the QoS of $S_2$ is zero when it is fully subscribed ($\lambda_2 = 1$), which is equivalent to the parameter setting $c = \overline{q}/(1 - l)$. Then the revenue maximization problem can be expressed as

$$\underset{p_1,p_2}{\text{maximize}}\ R = p_1\lambda_1^*(p_1, p_2) + p_2\lambda_2^*(p_1, p_2) \tag{5.37}$$

The optimal solution to problem (5.37) is summarized in the following theorem.

**Theorem 5.** In a duo-service monopoly market with two types of services $S_1$ and $S_2$, the QoS pair is $(q_1, q_2(\lambda_2))$, satisfying $p_1 > p_2$ and $q_1 > q_2(\lambda_2)$ for all $\lambda_2 \in [0, 1]$. Assume that the QoS valuation parameter $\theta$ is uniformly distributed and the subscribers make rational decision according to (5.29), then the maximum revenue is reached when $p_1^\dagger = q_1/2,\ p_2^\dagger \geq \overline{q}_2/2,\ \lambda_1^\dagger = 1/2,\ \lambda_2^\dagger = 0,$ and $R^{\max} = q_1/4$.

The proof is as follows.

Proof: Depending on the fraction of subscribers to $S_2$, the revenue of the CSP will have different forms, which necessitates a complete discussion on all the possible combinations. In what follows, we partition the domain of price selections into three disjoint cases, each of which is solved individually. The result of Theorem 5 is proved by summarizing the results

from all the three cases.

*Case 1* $\left(\text{if } \frac{p_1}{q_1} < \frac{p_2}{\overline{q}_2}\right)$: In this case, no user would subscribe to service $S_2$ since $S_1$ provides a superior service at a lower price. Thus, the revenue is solely contributed by $S_1$, which is given by

$$R = p_1 \cdot \lambda_1^* = p_1 \left(1 - \frac{p_1}{q_1}\right). \tag{5.38}$$

Then, the revenue maximization problem can be written as

$$\begin{aligned} \underset{p_1}{\text{maximize}} \quad & R = -\tfrac{p_1^2}{q_1} + p_1 \\ \text{subject to} \quad & \tfrac{p_1}{q_1} < \tfrac{p_2}{\overline{q}_2} \end{aligned} \tag{5.39}$$

with the optimal solution given by $p_1^\dagger = q_1/2, p_2^\dagger > \overline{q}_2/2$, and $R_{max} = q_1/4$.

*Case 2* $\left(\text{if } \frac{p_1}{q_1} \geq \frac{p_2}{\overline{q}_2} \text{ and } \frac{p_1 - p_2}{q_1 - \overline{q}_2} - \frac{p_2}{\overline{q}_2} \leq l\right)$: In this case, $S_2$ provides an affordable price and some users would subscribe to $S_2$, which is stabilized at an unsaturated state. Based upon (5.29), the revenue is obtained as

$$\begin{aligned} R &= p_1 \cdot \lambda_1^* + p_2 \cdot \lambda_2^* \\ &= p_1 \left[1 - F\left(\tfrac{p_1 - p_2}{q_1 - \overline{q}_2}\right)\right] + p_2 \left[F\left(\tfrac{p_1 - p_2}{q_1 - \overline{q}_2}\right) - F\left(\tfrac{p_2}{\overline{q}_2}\right)\right], \end{aligned} \tag{5.40}$$

which leads to a convex optimization problem

$$\begin{aligned} \underset{p_1, p_2}{\text{maximize}} \quad & p_1 \left(1 - \tfrac{p_1 - p_2}{q_1 - \overline{q}_2}\right) + p_2 \left(\tfrac{p_1 - p_2}{q_1 - \overline{q}_2} - \tfrac{p_2}{\overline{q}_2}\right) \\ \text{subject to} \quad & \tfrac{p_1}{q_1} \geq \tfrac{p_2}{\overline{q}_2}, \tfrac{p_1 - p_2}{q_1 - \overline{q}_2} - \tfrac{p_2}{\overline{q}_2} \leq l. \end{aligned} \tag{5.41}$$

The optimal solution is given by $p_1^\dagger = q_1/2, p_2^\dagger = \overline{q}_2/2$, and $R_{max} = q_1/4$.

*Case 3* $\left(\text{if } \frac{p_1 - p_2}{q_1 - \overline{q}_2} - \frac{p_2}{\overline{q}_2} > l\right)$: In this case, $S_2$ offers a much more attractive price for a unit level of QoS provided. Therefore, in the equilibrium point, service $S_2$ is stabilized at a

saturated state. The optimal fraction of subscribers is the solution to the following equation

$$\lambda_2^* = F\left(\frac{p_1 - p_2}{q_1 - q_2(\lambda_2^*)}\right) - F\left(\frac{p_2}{q_2(\lambda_2^*)}\right), \tag{5.42}$$

the closed-form of which is mathematically difficult to solve. Utilizing the *generalized marginal user principle* [73], which is given by

$$\theta_1^* = F\left(\frac{p_1 - p_2}{q_1 - q_2(\lambda_2^*)}\right) \quad \text{and} \quad \theta_2^* = F\left(\frac{p_2}{q_2(\lambda_2^*)}\right), \tag{5.43}$$

an equivalent optimization problem in terms of the QoS valuation parameter $\theta$ can be formulated as

$$\begin{aligned} \underset{\theta_1^*,\theta_2^*}{\text{maximize}} \quad & (1-\theta_1^*)p_1^*(\theta_1^*,\theta_2^*) + (\theta_1^* - \theta_2^*)p_2^*(\theta_1^*,\theta_2^*) \\ \text{subject to} \quad & \tfrac{p_1^*(\theta_1^*,\theta_2^*) - p_2^*(\theta_1^*,\theta_2^*)}{q_1 - \bar{q}_2} - \tfrac{p_2^*(\theta_1^*,\theta_2^*)}{\bar{q}_2} > l, \end{aligned} \tag{5.44}$$

where

$$\begin{aligned} p_1^*(\theta_1^*,\theta_2^*) &= \theta_1^* q_1 - (\theta_1^* - \theta_2^*)\cdot q_2(\theta_1^* - \theta_2^*), \\ p_2^*(\theta_1^*,\theta_2^*) &= \theta_2^* \cdot q_2(\theta_1^* - \theta_2^*). \end{aligned} \tag{5.45}$$

The reformulated problem is still a non-convex problem. Nevertheless, three locally optimal solutions can be obtained by investigating the KKT conditions, where it can be shown that $(\theta_1^\dagger, \theta_2^\dagger) = (1/2, 1/2)$ is the only feasible solution, indicating that it is also a globally optimal solution, which completes the proof. ■

**Remark 3** – Theorem 5 basically states that the maximum revenue is solely contributed by the superior service class of $S_1$. In other words, the revenue-maximizing strategy for the CSP is to select a proper combination of the services prices $(p_1^\dagger, p_2^\dagger)$ such that no user would subscribe to $S_2$ and exactly half of the population opt for $S_1$. Specifically, to prevent users

from subscribing to $S_2$, the corresponding service price $p_2^\dagger$ should be no less than half of the highest QoS. Note that this somewhat surprising result is obtained when the QoS valuation parameter $\theta$ is uniformly distributed, and it would be interesting to study the impact of other subscriber models, i.e., normal distribution. While the above results maximize the revenue of the duo-class market, it only benefits half of the population, leaving the other half untended. This may not be a preferable situation, especially when one wants to promote a particular type of service or increase service penetrations. One such alternative is to maximize a weighted combination of the revenues from both types of services, i.e.,

$$\underset{p_1,p_2}{\text{maximize}} \quad \omega_1 p_1 \lambda_1^*(p_1,p_2) + \omega_2 p_2 \lambda_2^*(p_1,p_2), \tag{5.46}$$

where $\omega_1 \in [0,1]$ is the weight of $S_1$ and $\omega_2 = 1-\omega_1$ the weight of $S_2$. By adjusting the weight parameter $\omega_2$, the CSP changes the priorities that are associated with both types of services, achieving a desired tradeoff between revenue and service penetration.

We now provide the simulation results of this case by investigating the maximum revenue $R^{max}$ as a function of the transition point $l$ when the weight parameter $\omega_2$ increases in a duo-service market. In Fig. 5.4, the following observations are available. First, $R^{max}$ decreases monotonically as $w_2$ increases from 0.5 to 0.9. Secondly, the maximum revenue curve is non-increasing just as the one in the single service market. The investment is more effective for larger value of $\omega_2$, i.e., when more priority (large weight) is given to $S_2$. Depending on the position of $\lambda_2^*$, the maximum revenue curve $R^{\max}$ is split into two sections by the turning point. These observations can assist the CSP in achieving a desirable tradeoff between monetization and customer acquisition. Finally, we plot in Fig. 5.5 the custom acquisition rate as a function of the weight parameter of $\omega_2$ for the weighted optimization approach. As more priority is given to $S_2$, the corresponding share of subscribers to $S_1$ (i.e., $\lambda_1^\dagger$) drops monotonically. Nevertheless, we observe that by adjusting weights between the two services,

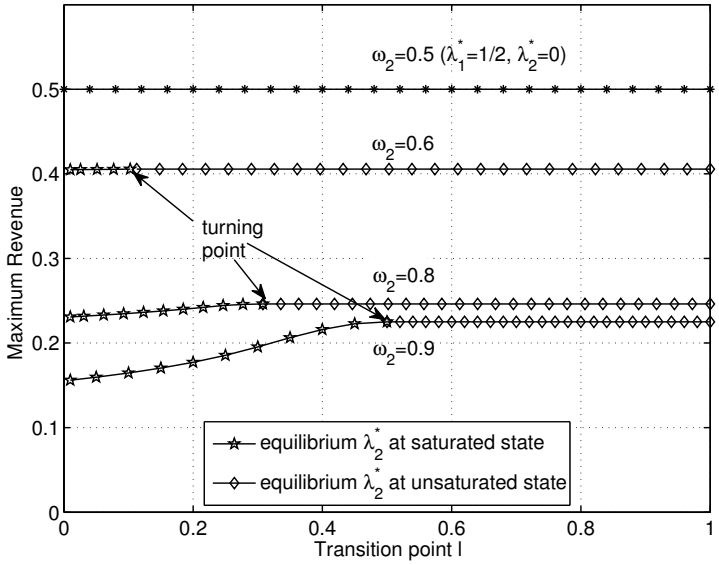


Figure 5.4: Maximum revenue $R^{max}$ in a duo-service market using weighted revenue maximization with weight $\omega_2 \in \{0.5, 0.6, 0.8, 0.9\}$, $q_1 = 4$ and $\bar{q}_2 = 1$.

the CSP achieves a higher overall custom acquisition rate (i.e., $\lambda_1^\dagger + \lambda_2^\dagger$) no smaller than 0.5.

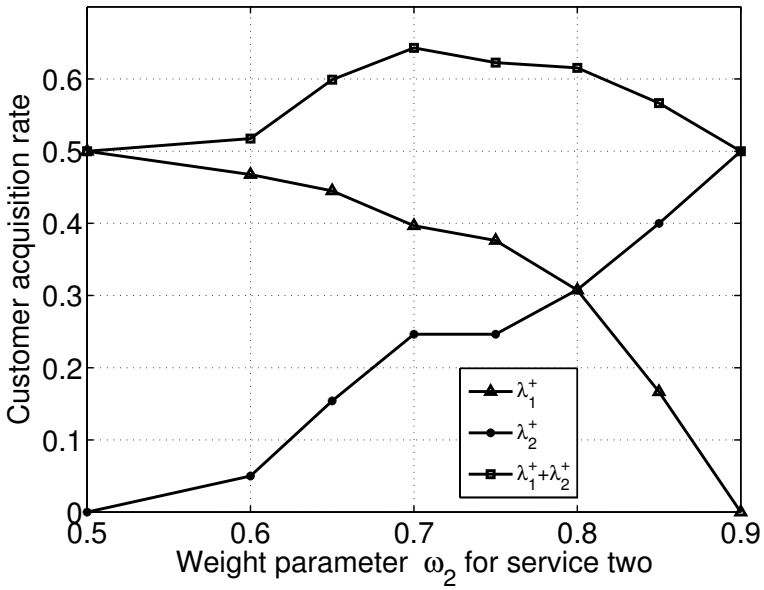


Figure 5.5: Customer acquisition rate in a duo-service market using weighted revenue maximization with weight $\omega_2 \in [0.5, 0.9]$ (with $\omega_2$ being the weight parameter of $S_2$, and $\lambda_1^\dagger, \lambda_2^\dagger$ the revenue-maximizing fraction of subscribers to $S_1$ and $S_2$, respectively.)

## 5.5 Conclusion

The optimal operating strategies in future PHEV charging service markets have been addressed in this chapter. By considering a single-service market with a piecewise QoS function, existing works have been generalized to encompass the case of semi-differentiable QoS models. By resorting to the concept of subdifferential, we have addressed the important issues of existence and uniqueness of the subscriber dynamics as well as its convergence. This part of the result has been strengthened next by the exemplary study of a parallel battery charging model in a PHEV charging service market. Next, the issue of revenue maximization in a duo-service market is studied and the optimal pricing strategies that maximize the revenue generated from both classes of services are derived. Finally, we have shown that the CSP can achieve balanced revenue generation and service penetration can be achieved through a weighted revenue maximization approach.

# Chapter 6

# Conclusions and Further Research Issues

## 6.1 Conclusions

In this dissertation, we have discussed various aspects of scheduling and pricing optimization problems in the smart grid, such as the unit commitment, estimation of the renewable source of wind power, resource allocation, service restoration problems in the microgrid and revenue-maximizing pricing strategies in a PHEV charging service market.

- The study of operation scheduling in the microgrid develops a new method for an economic and environmental driven UC problem in distributed resources island systems. The convex transformation of the original problem is a key point for a closed form solution. Simulation results have shown the accuracy and efficiency of the proposed method. Besides, the proposed method provides guidelines in deciding the size of the distributed resources, such as the ESS, to improve the self-sufficiency of the microgrid.

- The proposed method has been modified to incorporate the interconnection with the main grid. The revised new problem is still convex and a closed form solution is

also obtained. The realization of this interaction not only improves the stability of microgrid, but also benefits the full use of energy for both microgrid and macrogrid.

- The service restoration problem with uncertainties from both wind power and the duration of the breakdown in a microgrid has been investigated. The proposed two methods provide sub-optimal yet efficient solutions to the original problem. Compared to the classic progressive hedging method, the proposed methods save a lot of computation and complexity. The methods also provide guidelines to microgrid design, e.g., the capacity of the ESS and configuration strategies of the power network.

- The results in Chapter 5 indicate that, on one hand, although the service provider provides two types of services, $S_1$ contributes more to the system revenue than $S_2$. In other words, $S_1$ will be a primary service if the service provider intends to maximize revenue and achieve better control of the grid. On the other hand, although $S_2$ does little help in maximizing system revenue, it plays an important role in the better use of the special power line and increasing the social welfare. This is meaningful for the CSP and could improve the spread of PHEVs.

## 6.2 Further Research Issues

There are many open issues for further research in the topics we discussed in the dissertation.

- The work of operation scheduling in a microgrid (islanded mode) can be extended in several directions. First, in the UC problem we have not considered the theoretical analysis of the ESS, but provided the simulation result showing that the ESS is necessary for the integration of wind power generation to absorb the extra energy and compensate for the expected energy that is not be served by the wind turbines. In the future work, one more study should focus on the theoretical analysis for the ESS. Sec-

ond, we could also extend the PSS idea other renewable resources, such as solar-power, which is also envisioned as a critical DER in the grid.

- For the work on a microgrid in connected mode, we have the following direction for further research. Energy waste becomes a common problem for different nations, especially the electricity energy. If the interactions between the macrogrid and microgrid, or among microgrids, are realized, our community would benefit from the full use of the energy. The optimal price of purchasing and selling from and to the main grid should be considered. If the price is too low, the microgrid would rather purchase all the energy from the main grid than generate it itself, which leads to resource under-utilization in the microgird, and vice versa.

- For the service restoration problem in Chapter 4, there are some open issues left. In the simulation part, pu values are used to reveal the relation between the capacity of the ESS and wind power generation. However, it would be more meaningful to put pu values in the entire system to reveal the relations among all distributed generators. Second, the proposed method can be put into practice in a real power network; the study on the power and energy flow would be instructive for the microgrid design and service restoration operation.

- While our analysis in Chapter 5 focuses only on revenue maximization for the CSP and the provided social welfare, respectively, the future work could be in the tradeoff between them. Moreover, as in a duopoly market, the competition among many CSPs will be meaningful and interesting, and contributes more to the development of the PHEV charging service market in the future.

# Bibliography

[1] A. Cohen and V. Sherkat, "Optimization-based methods for operations scheduling," *Proc. IEEE*, vol. 75, pp. 1574–1591, Dec. 1987.

[2] N. Padhy, "Unit commitment-a bibliographical survey," *IEEE Trans. Power Syst.*, vol. 19, pp. 1196–1205, May 2004.

[3] S. A. Pourmousavi, M. H. Nehrir, C. M. Colson, and C. Wang, "Real-time energy management of a stand-alone hybrid wind-microturbine energy system using particle swarm optimization," *IEEE Trans. Sustainable Energy*, vol. 1, pp. 193–201, Oct. 2011.

[4] R. Yinger, "Behavior of capstone and honeywell microturbine generators during load changes," tech. rep., California Energy Commission, 2001.

[5] C. Hernandez, T. Green, and N. Mugniot, "Fuel consumption minimization of a microgrid," *IEEE Trans. Ind. Appl.*, vol. 41, pp. 673–681, May 2005.

[6] C. Chen, S. Duan, T. Cai, B. Liu, and G. Hu, "Smart energy management system for optimal microgrid economic operation," *IET Renewable Power Generation*, vol. 5, pp. 258–267, May 2011.

[7] T. Logenthiran and D. Srinivasan, "Short term generation scheduling of a microgrid," in *Proc. IEEE TENCON*, pp. 1–6, Nov. 2009.

[8] M. R. Alrashidi and M. E. El-Hawary., "Impact of loading conditions on the emission-economic dispatch," *Proc. World Academy of Science, Engineering and Technology*, vol. 2, no. 9, pp. 148–151, 2008.

[9] R. Brown, S. Gupta, R. Christie, S. Venkata, and R. Fletcher, "Automated primary distribution system design: reliability and cost optimization," (Los angeles, USA), pp. 1–6, Nov. 1996.

[10] S. Jonnavithula and R. Billinton, "Minimum Cost Analysis of Feeder Routing in Distribution System Planning," *IEEE Transactions on Power Delivery*, vol. 11, pp. 1935–1940, Oct. 1996.

[11] Y. Tang, "Power Distribution System Planning with Reliability Modeling and Optimization," *IEEE Transactions on Power Systems*, vol. 11, pp. 181–189, Feb. 1996.

[12] S. Chen, H. Gooi, and M. Wang, "Sizing of energy storage for microgrids," *IEEE Trans. Smart Grid*, vol. 3, pp. 142–151, Mar. 2012.

[13] A. Abdollahi, M. P. Moghaddam, M. Rashidinejad, and M. K. Sheikh-El-Eslami, "Investigation of economic and environmental-driven demand response measures incorporating UC," *IEEE Trans. Smart Grid*, vol. 3, pp. 12–25, Mar. 2012.

[14] A. Hawkes and M. Leach, "Modelling high level system design and unit commitment for a microgrid," *Appl. Energy*, vol. 86, pp. 1253–1265, July 2009.

[15] I. Gradshteyn and I. Ryzhik, *Table of Integrals, Series, and Products*. Elsevier, seventh ed.

[16] H. Feroze, *Multi-agent systems in microgrids: Design and implementation*. Master thesis, Virginia Polytechnic Institute and State University, 2009.

[17] L. Tao and C. Schwaegerl, "Advanced architectures and control concepts for more microgrids," tech. rep., European Commission Project, 2009.

[18] M. Pipattanasomporn, H. Feroze, and S. Rahman, "Securing critical loads in a PV-based microgrid with a multi-agent system," *Renewable Energy*, vol. 39, pp. 166–174, Mar. 2012.

[19] J. Carta, P. Ramírez, and S. Velázquez, "A review of wind speed probability distributions used in wind energy analysis," *Renewable and Sustainable Energy Rev.*, vol. 13, pp. 933–955, June 2009.

[20] S. Roy, "Market constrained optimal planning for wind energy conversion systems over multiple installation sites," *IEEE Trans. Energy Convers.*, vol. 17, pp. 124–129, Mar. 2002.

[21] F. Barbir and T. Gómez, "Efficiency and economics of proton exchange membrane (PEM) fuel cells," *Int. J. Hydrogen Energy*, vol. 22, no. 10, pp. 1027–1037, 1997.

[22] F. Mohamed, *Microgrid modelling and online management*. PhD thesis, Helsinki University of Technology, 2008.

[23] A. Azmy and I. Erlich, "Online optimal management of PEM fuel cells using neural networks," *IEEE Trans. Power Del.*, vol. 20, pp. 1051–1058, Apr. 2005.

[24] J. L. Bernal-Agustín and R. Dufo-López, "Economical and environmental analysis of grid connected photovoltaic systems in Spain," *Renewable Energy*, vol. 31, pp. 1107–1128, July 2006.

[25] F. Mohamed and H. Koivo, "Multiobjective optimization using modified game theory for online management of microgrid," *Euro. Trans. Electr. Power*, vol. 21, pp. 839–854, Sept. 2011.

[26] A. Saber and G. Venayagamoorthy, "Plug-in vehicles and renewable energy sources for cost and emission reductions," *IEEE Trans. Ind. Electron.*, vol. 58, pp. 1229–1238, Mar. 2011.

[27] R. Doherty and M. O'Malley, "A new approach to quantify reserve demand in systems with significant installed wind capacity," *IEEE Trans. Power Syst.*, vol. 20, no. 2, pp. 587–595, 2005.

[28] S. Tewari, C. J. Geyer, and N. Mohan, "A statistical model for wind power forecast error and its application to the estimation of penalties in liberalized markets," *IEEE Trans. Power Syst.*, vol. 26, pp. 2031–2039, Nov. 2011.

[29] S. Boyd and L. Vandenberghe, *Convex Optimization*. Cambridge University Press, 2004.

[30] D. P. Bertsekas, *Nonlinear Programming*. Athena Scientific, 1995.

[31] "Wind Energy Database of White Deer." `http://www.windenergy.org/datasites/14-whitedeer/`, Date: 2014.09.19.

[32] A. Tsikalakis and N. Hatziargyriou, "Centralized control for optimizing microgrids operation," *IEEE Trans. Energy Conversion*, vol. 23, pp. 241–248, Feb. 2011.

[33] T. Nagata and H. Sasaki, "An efficient algorithm for distribution network restoration," vol. 1, (Vancouver, Canada), pp. 54–59, 2001.

[34] R. Masiello and S. Venkata, "Microgrids-there may be one in your future," *IEEE Power Energy Mag.*, vol. 11, pp. 14–93, June 2013.

[35] "IEEE Guide for Design, Operation, and Integration of Distributed Resource Island Systems with Electric Power Systems," Tech. Rep. July, IEEE Std 1547.4, 2011.

[36] "Smart Grid Research and Development Multi-Year Program Plan (2010-2014)," Tech. Rep. Sep, 2012.

[37] H. Laaksonen and K. Kauhaniemi, "Control principles for blackstart and island operation of microgrid," in *Proc. of the Nordic Workshop on Power and Ind. Electron.*, (Espoo, Finland), pp. 1–7, June 2008.

[38] L. Fink, K. Liou, and C. Liu, "From generic restoration actions to specific restoration strategies," *IEEE Trans. on Power Syst.*, vol. 10, pp. 745–752, May 1995.

[39] "American National Standard for Electric Power Systems and EquipmentVoltage Ratings (60 Hertz)," tech. rep., ANSI C84.1, 2011.

[40] "IEEE Draft Standard for Interconnecting Distributed Resources with Eletric Power Systems," tech. rep., IEEE WG Std. 1547-2003, 2001.

[41] J. A. Lopes, C. L. Moreira, and A. G. Madureira, "Defining control strategies for microgrids islanded operation," *IEEE Trans. Power Syst.*, vol. 21, pp. 916–924, May 2006.

[42] Y. Mao and K. Miu, "Switch placement to improve system reliability for radial distribution systems with distributed generation," *IEEE Trans. Power Syst.*, vol. 18, pp. 1346–1352, Nov. 2003.

[43] S. Thale and V. Agarwal, "A smart control strategy for the black start of a microgrid based on PV and other auxiliary sources under islanded condition," in *IEEE Photovoltaic Specialists Conf.*, (Seattle, WA), pp. 2454–2459, 2011.

[44] C. Moreira, F. Resende, and J. Lopes, "Using low voltage microgrids for service restoration," *IEEE Trans. Power Syst.*, vol. 22, pp. 395–403, Jan. 2007.

[45] Y. Fukuyama and H. Endo, "A hybrid system for service restoration using expert system and genetic algorithm," in *IEEE int. conf. Intelligent Syst. Applicat. to Power Syst.*, (Orlando, FL), pp. 3–7, 1996.

[46] Y. Hsu and H. Huang, "Distribution system service restoration using the artificial neural network approach and pattern recognition method," *IEEE proc. Gener. Transm. Distrib.*, vol. 142, pp. 1–5, May 1995.

[47] J. Momoh and A. Caven, "Distribution system reconfiguration scheme using integer interior point programming technique," in *IEEE PES Transmission and Distribution Conf. and Exposition*, vol. 1, (Acapulco, Mexico), pp. 234–241, 2003.

[48] R. Pérez-guerrero, G. T. Heydt, N. J. Jack, B. K. Keel, and A. R. C. Castelhano, "Optimal restoration of distribution systems using dynamic programming," *IEEE Trans. Power Delivery*, vol. 23, pp. 1589–1596, June 2008.

[49] R. Rockafellar and R. Wets, "Scenarios and policy aggregation in optimization under uncertainty," *Mathematics of Operations Research*, vol. 16, pp. 119–147, Feb. 2008.

[50] M. Pipattanasomporn, H. Feroze, and S. Rahman, "Multi-agent systems in a distributed smart grid: Design and implementation," (Seattle, WA), pp. 1–8, IEEE, Mar. 2009.

[51] K. Michael, "Wind speed data and its application to wind generated power," *Homepower*, vol. 62, pp. 34–38, Jan. 1997.

[52] T. Nagata and H. Sasaki, "An efficient algorithm for distribution network restoration," in *Power Eng. Soc. Summer Meeting*, (Vancouver, BC), pp. 54–59, 2001.

[53] H. Chiang and R. Jumeau, "Optimal network reconfigurations in distribution systems II: Solution algorithms and numerical results," *IEEE Trans. Power Delivery*, vol. 5, no. 3, pp. 1568–1574, 1990.

[54] C. Su and C. Lee, "Network reconfiguration of distribution systems using improved mixed-integer hybrid differential evolution," *IEEE Trans. Power Delivery*, vol. 18, pp. 1022–1027, July 2003.

[55] A. Zidan and E. El-Saadany, "A cooperative multiagent framework for self-healing mechanisms in distribution systems," *IEEE Trans. Smart Grid*, vol. 3, no. 3, pp. 1525–1539, 2012.

[56] J. Mulvey and A. Ruszczynski, "A new scenario decomposition method for large-scale stochastic optimization," *Operations Research*, vol. 43, pp. 477–490, June 1995.

[57] Z. Chen, S. Li, and D. Tirupati, "A scenario-based stochastic programming approach for technology and capacity planning," *Computers and Operations Research*, vol. 29, pp. 781–806, June 2002.

[58] L. Tang, P. Che, and J. Wang, "Corrective unit commitment to an unforeseen unit breakdown," *IEEE Trans. on Power Syst.*, vol. 27, pp. 1729–1740, Apr. 2012.

[59] S. Takriti and J. Birge, "Lagrangian solution techniques and bounds for loosely coupled mixed-integer stochastic programs," *Operations Research*, vol. 48, pp. 91–98, Feb. 2000.

[60] B. Zhao, Y. Shi, X. Dong, W. Luan, and J. Bornemann, "Short-term operation scheduling in renewable-powered microgrids: A duality-based approach," *IEEE Trans. Sustainable Energy*, vol. 5, pp. 209–217, Jan. 2013.

[61] J. Muckstadt and S. Koenig, "An application of lagrangian relaxation to scheduling in power-generation systems," *Operations Research*, vol. 25, pp. 387–403, May 1977.

[62] S. Civanlar, J. Grainger, H. Yin, and S. Lee, "Distribution feeder reconfiguration for loss reduction," *IEEE Trans. Power Delivery*, vol. 3, pp. 1217–1223, July 1988.

[63] T. Ou, W. Lin, C. Huang, and F. Cheng, "A hybrid programming for distribution reconfiguration of dc microgrid," in *IEEE PES Conf. on Sustainable Alternative Energy*, (Valencia), pp. 1–7, 2009.

[64] "Cairngorm Automatic Weather Station." http://cairngormweather.eps.hw.ac.uk/archive.htm, Date: 2014.09.19.

[65] J. Watson, D. L. Woodruff, and D. R. Strip, "Progressive hedging innovations for a class of stochastic resource allocation problems," *Comutational Management Science*, vol. 8, pp. 355–370, Nov. 1997.

[66] K. Morrow, D. Karner, and J. Francfort, "Plug-in hybrid electric vehicle charging infrastructure review," Tech. Rep. 58517, The Idah National Laboratory, 2008.

[67] A. Senart, S. Kurth, and G. Le Roux, "Assessment framework of plug-in electric vehicles strategies," in *Proc. IEEE Int. Conf. Smart Grid Commun.*, (Gaithersburg, MD), pp. 155–160, 2010.

[68] "China Opens Largest EV charging station." http://goelectricdrive.com/index.php/news-events/item/97-china-opens-largest-ev-charging-station, Date: 2014.09.19.

[69] M. M. Collins and G. H. Mader, "The timing of EV recharging and its effect on utilities," *IEEE Trans. Veh. Technol.*, vol. 32, pp. 90–97, Dec. 1983.

[70] A. Ipakchi and F. Albuyeh, "Grid of the future," *IEEE Power Energy*, vol. 7, pp. 52–62, Feb. 2009.

[71] Y. Liu, R. Xu, and T. Chen, "Investigation on the construction mode of the charging station and battery-swap station," in *IEEE Electric Inform. and Control Eng. (ICE-ICE)*, (Wuhan, China), pp. 5080–5081, 2011.

[72] "EDF and Toyota Announce Large-scale Emonstration of PHEV in Strasboug, France.." http://press.edf.com/press-42871.html, Date: 2014.09.19.

[73] D. Acemoglu, A. Ozdaglar, and R. Srikant, "The marginal user principle for resource allocation in wireless networks," in *Proc. IEEE Conf. on Decision and Control (CDC)*, pp. 1544–1549, 2004.

[74] C. Chau, Q. Wang, and D. Chiu, "On the viability of Paris metro pricing for communication and service networks," in *Proc. IEEE Conf. Comput. Commun. (INFOCOM)*, (San Diego, CA), 2010.

[75] S. Ren, J. Park, and M. Van Der Schaar, "User subscription, revenue maximization, and competition in communications markets," in *Proc. IEEE Conf. Comput. Commun. (INFOCOM)*, (Shanghai, China), pp. 2696–2704, 2011.

[76] C. K. Alexander and N. O. S. Mathew, *Fundamentals of Electric Circuits*. New York: Mcgraw Hill Higher Education, 3rd ed., 2006.

[77] M. Erol-Kantarci, J. Sarker, and H. Mouftah, "Analysis of plug-in hybrid electrical vehicle admission control in the smart grid," in *Proc. IEEE Int. Workshop Comput. Aided Modeling and Design Commun. Links and Netw.*, (Denver, CO), pp. 56–60, 2011.

[78] "Charging Lithium ion." `http://batteryuniversity.com/learn/article/charging_lithium_ion_batteries`, Date: 2014.09.19.